*J Antimicrob Chemother* 2014; **69**: 1385–1389
doi:10.1093/jac/dkt514 Advance Access publication 29 December 2013

Journal of Antimicrobial Chemotherapy

# Cumulative exposure to ritonavir-boosted atazanavir is associated with cholelithiasis in patients with HIV-1 infection

**Takeshi Nishijima[1,2], Takuro Shimbo[3], Hirokazu Komatsu[4], Yohei Hamada[1], Hiroyuki Gatanaga[1,2]*, Yoshimi Kikuchi[1] and Shinichi Oka[1,2]**

*[1]AIDS Clinical Center, National Center for Global Health and Medicine, Tokyo, Japan; [2]Center for AIDS Research, Kumamoto University, Kumamoto, Japan; [3]Department of Clinical Study and Informatics, Center for Clinical Sciences, National Center for Global Health and Medicine, Tokyo, Japan; [4]Department of Community Care, Saku Central Hospital, Nagano, Japan*

*Corresponding author. AIDS Clinical Center, National Center for Global Health and Medicine, 1-21-1, Toyama, Shinjuku-ku, Tokyo 162-8655, Japan. Tel: +81-3-3202-7181; Fax: +81-3-3208-4244; E-mail: higatana@acc.ncgm.go.jp

*Received 20 September 2013; returned 25 November 2013; revised 26 November 2013; accepted 7 December 2013*

**Objectives:** This study aimed to examine the effect of long-term treatment with ritonavir-boosted atazanavir (atazanavir/ritonavir) on cholelithiasis.

**Methods:** A single-centre, cross-sectional study was conducted to elucidate the prevalence of cholelithiasis in patients with HIV-1 infection who underwent abdominal ultrasonography between January 2004 and March 2013. Univariate and multivariate logistic regression analyses were applied to estimate the effects of >2 years of atazanavir/ritonavir exposure on cholelithiasis as the primary exposure.

**Results:** Of the 890 study patients, 84 (9.4%) had >2 years of atazanavir/ritonavir exposure. Cholelithiasis was twice as frequent in those treated for >2 years with atazanavir/ritonavir [15 (18%) of 84 patients] compared with those treated for <2 years [72 (8.9%) of 806 patients] ($P=0.018$). Univariate analysis showed a significant association between >2 years of atazanavir/ritonavir exposure and cholelithiasis (OR=2.216; 95% CI=1.206–4.073; $P=0.010$) and the association almost persisted in multivariate analysis (adjusted OR=1.806; 95% CI=0.922–3.537; $P=0.085$). Long-term treatment (>2 years) with other commonly used protease inhibitors, such as ritonavir-boosted lopinavir and ritonavir-boosted darunavir, was not associated with cholelithiasis in univariate and multivariate analysis. Additional analysis showed that >1 year of exposure to atazanavir/ritonavir was significantly associated with cholelithiasis (OR=1.857; 95% CI=1.073–3.214; $P=0.027$), whereas >1 year of exposure to ritonavir-boosted lopinavir and ritonavir-boosted darunavir was not.

**Conclusions:** Long-term treatment of patients with HIV-1 infection for >2 years with atazanavir/ritonavir was associated with an increased risk of cholelithiasis compared with patients with shorter exposure. Long-term exposure to atazanavir/ritonavir appears to increase the risk of cholelithiasis in patients with HIV-1 infection.

**Keywords:** protease inhibitors, antiretroviral therapy, gallstones

## Introduction

Ritonavir-boosted atazanavir (atazanavir/ritonavir) is a widely used protease inhibitor in the treatment of patients infected with HIV-1.[1–3] Cholelithiasis was not reported in atazanavir/ritonavir Phase 3 clinical trials;[4] however, recent post-marketing studies have suggested potential association between cumulative atazanavir/ritonavir exposure and cholelithiasis.[5–7] Only a couple of studies have so far reported the incidence of complicated cholelithiasis, such as cholecystitis, cholangitis and pancreatitis, in patients treated with atazanavir/ritonavir.[5,8] However, the effects of prolonged exposure to atazanavir/ritonavir on the incidence of cholelithiasis, including asymptomatic cholelithiasis, is unknown at this stage. This is of importance because ~20% of patients with cholelithiasis develop symptoms in the long term.[9]

The aim of this study was to elucidate the effects of atazanavir/ritonavir exposure on cholelithiasis, including asymptomatic cholelithiasis, in patients with HIV-1 infection.

## Patients and methods

### Study design

We performed a cross-sectional study of HIV-1-infected patients using the abdominal ultrasonography data and the medical records at the National Center for Global Health and Medicine, Tokyo, Japan.[10] The study

population was HIV-1-infected patients, aged >17 years, who underwent abdominal ultrasonography at the Physiological Examination Unit of the hospital between 1 January 2004 and 31 March 2013 as part of clinical practice. Atazanavir/ritonavir became available in Japan in January 2004. Exclusion criteria were: (i) patients with cholecystectomy performed before the study period; and (ii) patients with missing data on antiretroviral therapy (ART). At the Physiological Examination Unit, ultrasonography was conducted by certified medical technologists and the images and diagnosis were double-checked and confirmed by radiologists, hepatologists or gastroenterologists. If abdominal ultrasonography was conducted more than once during the study period, the latest ultrasonography data were used for the study. This study was approved by the Human Research Ethics Committee of the hospital. Each participant provided a written informed consent for the clinical and laboratory data to be used and published for research purposes.

### Measurements

The primary exposure variable was a history of atazanavir/ritonavir use for >2 years, regardless of continuation of atazanavir/ritonavir at the time of abdominal ultrasonography. A 2 years threshold for atazanavir/ritonavir exposure was selected because cholelithiasis was not reported in atazanavir/ritonavir Phase 3 clinical trials with the primary endpoint set at week 48[4] and prolonged excretion of atazanavir in the bile appears necessary for gallstone formation.[5] The potential risk factors for cholelithiasis were collected from the medical records, together with the basic demographics.[9,11–13] They included age, sex, ethnicity, body mass index (BMI), cirrhosis, diabetes mellitus, CD4 count, HIV viral load, ART experienced or naive, duration of ART, length of exposure to atazanavir/ritonavir, ritonavir-boosted lopinavir (lopinavir/ritonavir) and ritonavir-boosted darunavir (darunavir/ritonavir), history of AIDS and hepatitis B or C coinfection. We used data collected within 3 months of the day ultrasonography was conducted.

### Statistical analysis

Univariate and multivariate logistic regression analysis was used to estimate the effects of atazanavir/ritonavir exposure of >2 years, relative to <2 years or no atazanavir/ritonavir exposure, on cholelithiasis as the primary exposure. Basic demographics (age and sex), possible risk factors for cholelithiasis (BMI, cirrhosis and diabetes mellitus)[11–13] and variables with *P* values <0.05 in univariate analysis (HIV load and duration of ART) were added to the multivariate model. The variable 'treatment naive' was not added because of its multicollinearity with HIV load.

Statistical significance was defined as two-sided *P* values <0.05. We used ORs and 95% CIs to estimate the effects of each variable on cholelithiasis. All statistical analyses were performed with the Statistical Package for Social Sciences ver. 20.0 (SPSS, Chicago, IL, USA).

## Results

Of the 890 study patients, cholelithiasis was diagnosed by abdominal ultrasonography in 87 patients, with a prevalence of 9.8% (see Figure S1, available as Supplementary data at *JAC* Online). Patients with cholelithiasis were significantly older, more likely to be females, have lower HIV-1 viral load, be diabetic, have cirrhosis and have longer exposure to ART (Table 1). On the other hand, patients without cholelithiasis were more likely to be treatment naive.

Of the 890 study patients, 186 (21%) were treated with atazanavir for a median duration of 1.79 years (IQR 0.68–3.78 years) and 84 (9.4%) patients were treated with atazanavir for >2 years. Of the 186 patients treated with atazanavir, 173 (93%) patients were on atazanavir/ritonavir, whereas only 13 (7%) were on non-boosted atazanavir. Cholelithiasis was twice as frequent in patients treated for >2 years with atazanavir [15 (18%) of

**Table 1.** Basic demographics of total study patients, patients with cholelithiasis and no cholelithiasis

| | Total (*n*=890) | Cholelithiasis (*n*=87) | No cholelithiasis (*n*=803) | *P*[a] |
|---|---|---|---|---|
| Age, years[b] | 41 (35–50) | 45 (38–55) | 40 (34–49) | <0.001 |
| Female sex, *n* (%) | 49 (5.5) | 9 (10) | 40 (5) | 0.047 |
| Race (Asian), *n* (%) | 869 (98) | 87 (100) | 782 (97) | 0.253 |
| BMI, kg/m$^2$[b] | 21.9 (20.1–24.6) | 22.5 (20.1–25.7) | 21.8 (20–24.4) | 0.665 |
| CD4 cell count, cells/μL[b] | 365 (207–525) | 370 (226–572) | 365 (206–523) | 0.206 |
| HIV load, $\log_{10}$ copies/mL[b] | 1.70 (1.07–4.04) | 1.70 (1.70–1.90) | 1.70 (1.70–4.20) | 0.002 |
| HIV load <50 copies/mL, *n* (%) | 510 (57) | 64 (74) | 446 (56) | 0.001 |
| Diabetes mellitus, *n* (%) | 53 (6) | 10 (12) | 43 (5) | 0.030 |
| Hepatitis B or C coinfection, *n* (%) | 242 (27) | 23 (26) | 219 (27) | 1.000 |
| History of AIDS, *n* (%) | 298 (34) | 31 (36) | 267 (33) | 0.720 |
| Cirrhosis, *n* (%) | 14 (1.6) | 6 (7) | 8 (1) | 0.001 |
| Treatment naive, *n* (%) | 267 (30) | 14 (16) | 253 (32) | 0.003 |
| History of atazanavir/ritonavir exposure, *n* (%) | 186 (21) | 25 (29) | 161 (20) | 0.070 |
| History of lopinavir/ritonavir exposure, *n* (%) | 294 (33) | 32 (37) | 262 (33) | 0.472 |
| History of darunavir/ritonavir exposure, *n* (%) | 100 (11) | 13 (15) | 87 (11) | 0.281 |
| Duration of ART (years)[b] | 2.7 (0–7.9) | 4.8 (0.9–12) | 2.2 (0–7.4) | <0.001 |

Cirrhosis was diagnosed by abdominal ultrasonography, diabetes mellitus was defined by use of antidiabetic agents or fasting plasma glucose >126 mg/dL or plasma glucose >200 mg/dL on two different days, hepatitis B infection was defined by positive hepatitis B surface antigen and hepatitis C infection was defined by positive hepatitis C virus viral load.

[a]The $\chi^2$ test or Fisher's exact test was used for comparison of categorical data and Student's *t*-test was used for comparison of continuous variables.

[b]Median (IQR).

**Table 2.** Univariate and multivariate analysis to estimate the risk for cholelithiasis posed by long-term (>2 years) treatment with ritonavir-boosted atazanavir

| | Model 1, crude ($n$=890) | | | Model 2, adjusted ($n$=890) | | | Model 3, adjusted ($n$=851) | | |
|---|---|---|---|---|---|---|---|---|---|
| | OR | 95% CI | $P$ | OR | 95% CI | $P$ | OR | 95% CI | $P$ |
| >2 years of atazanavir/ritonavir exposure | 2.216 | 1.206-4.073 | 0.010 | 2.096 | 1.131-3.883 | 0.019 | 1.806 | 0.922-3.537 | 0.085 |
| Age per 1 year increment | 1.034 | 1.016-1.053 | <0.001 | 1.009 | 0.980-1.039 | 0.001 | 1.028 | 1.008-1.049 | 0.005 |
| Female sex | 2.201 | 1.030-4.705 | 0.042 | 2.005 | 0.921-4.368 | 0.080 | 2.183 | 0.986-4.834 | 0.054 |
| BMI per 1 kg/m$^2$ increment | 1.004 | 0.985-1.024 | 0.673 | | | | 1.001 | 0.983-1.020 | 0.881 |
| Cirrhosis | 7.361 | 2.493-21.74 | <0.001 | | | | 6.947 | 2.133-22.63 | 0.001 |
| Diabetes mellitus | 2.295 | 1.110-4.748 | 0.025 | | | | 1.017 | 0.417-2.481 | 0.971 |
| CD4 count per 1 cell/μL increment | 1.001 | 1.000-1.001 | 0.206 | | | | | | |
| HIV viral load per $\log_{10}$/mL increment | 0.748 | 0.618-0.906 | 0.003 | | | | 0.900 | 0.717-1.129 | 0.363 |
| History of AIDS | 1.111 | 0.700-1.765 | 0.655 | | | | | | |
| Treatment naive | 0.417 | 0.231-0.753 | 0.004 | | | | | | |
| Hepatitis B or hepatitis C coinfection | 0.958 | 0.581-1.582 | 0.868 | | | | | | |
| Duration of ART per 1 year increment | 1.077 | 1.040-1.115 | <0.001 | | | | 1.030 | 0.983-1.080 | 0.216 |

Model 1 was the univariate analysis to estimate the risk of various factors for cholelithiasis for atazanavir/ritonavir exposure of >2 years, relative to <2 years or no atazanavir/ritonavir exposure. In Model 2, atazanavir/ritonavir exposure of >2 years, relative to <2 years or no atazanavir/ritonavir exposure, was adjusted by adding age and sex. In Model 3, possible risk factors for cholelithiasis (BMI, cirrhosis and diabetes mellitus) and variables with $P$ values <0.05 in Model 1 (HIV load and duration of ART) were added. The variable 'treatment naive' was not added because of its multicollinearity with HIV load.

84 patients] compared with patients with no or <2 years of atazanavir [72 (8.9%) of 806 patients] ($P$=0.018).

Univariate analysis showed a significant association between >2 years of atazanavir/ritonavir exposure and cholelithiasis (OR=2.216; 95% CI=1.206-4.073; $P$=0.010) (Table 2, Model 1). Older age, female sex, cirrhosis, diabetes mellitus, low HIV viral load and duration of ART per 1 year increment were also significantly associated with cholelithiasis.

Multivariate analysis identified >2 years of atazanavir/ritonavir exposure as an independent risk factor for cholelithiasis after adjustment for age and female sex (adjusted OR=2.096; 95% CI=1.131-3.883; $P$=0.019) (Table 2, Model 2). The association was marginally significant after adjustment for other variables (adjusted OR=1.806; 95% CI=0.922-3.537; $P$=0.085) (Table 2, Model 3). Older age and cirrhosis also persisted in being significantly associated with cholelithiasis in multivariate analysis (age per 1 year increment, adjusted OR=1.028; 95% CI=1.008-1.049; $P$=0.005) (cirrhosis, adjusted OR=6.947; 95% CI=2.133-22.63; $P$=0.001).

Additional analyses focusing on the impact of other commonly used protease inhibitors demonstrated that 148 (16.6%) patients were treated with lopinavir/ritonavir for >2 years, while 29 (3.3%) were treated with darunavir/ritonavir for >2 years. Treatment for >2 years with lopinavir/ritonavir and darunavir/ritonavir was not associated with cholelithiasis in univariate and multivariate analysis adjusted with the same variables in Table 2, Model 3 (lopinavir/ritonavir: OR=1.246; 95% CI=0.710-2.185; $P$=0.443/adjusted OR=1.221; 95% CI=0.674-2.214; $P$=0.510) (darunavir/ritonavir: OR=1.067; 95% CI=0.316-3.601; $P$=0.916/adjusted OR=0.641; 95% CI=0.173-2.377; $P$=0.506). In univariate analysis, treatment for >1 year with atazanavir/ritonavir [$n$=124 (13.9%)] was also significantly associated with cholelithiasis (OR=1.857; 95% CI=1.073-3.214; $P$=0.027), whereas >1 year exposure to lopinavir/ritonavir [$n$=199 (22.4%)] and darunavir/ritonavir [$n$=53 (6%)] did not correlate with cholelithiasis (lopinavir/ritonavir: OR=1.367; 95% CI=0.830-2.252; $P$=0.220) (darunavir/ritonavir: OR=0.961; 95% CI=0.375-2.464; $P$=0.934).

## Discussion

To our knowledge, this is the first study to investigate the effects of atazanavir/ritonavir exposure on cholelithiasis, including asymptomatic cholelithiasis. Patients treated for >2 years with atazanavir/ritonavir were twice as likely to develop cholelithiasis compared with patients with no or <2 years of atazanavir/ritonavir exposure. Univariate analysis demonstrated a significant association between >2 years of atazanavir/ritonavir exposure and cholelithiasis (OR=2.216; 95% CI=1.206-4.073; $P$=0.010) and the association almost persisted in multivariate analysis (adjusted OR=1.806; 95% CI=0.922-3.537; $P$=0.085) (Table 2). Thus, long-term treatment with atazanavir/ritonavir was associated with cholelithiasis in this cohort. On the other hand, exposure to lopinavir/ritonavir or darunavir/ritonavir, other widely prescribed protease inhibitors, was not associated with cholelithiasis.

Two mechanisms are suggested for the observed atazanavir-induced cholelithiasis. First, precipitation of atazanavir in the bile might enhance the formation of calculi composed of atazanavir and other biliary components. This hypothesis is supported by the documentation of atazanavir as a component of gallstones in several case reports.[5-7] Strong acidity (e.g. pH of 1.9) is required to achieve optimal dissolution of atazanavir, whereas biliary pH is usually >6.5.[4] This feature of atazanavir might result in precipitation of atazanavir and consequent cholelithiasis.[4] It is well known that atazanavir/ritonavir is a risk factor for nephrolithiasis[14,15] and, recently, a case of atazanavir-containing sialolithiasis in a patient treated with atazanavir/ritonavir was also reported.[16] These data further support the likelihood of atazanavir involvement in lithiasis. Second, because atazanavir is a competitive

inhibitor of uridine diphosphate glucuronyl transferase 1A1 (UGT1A1), a bilirubin-conjugating enzyme, atazanavir is known to cause hyperbilirubinaemia.[17] This might result in a rise in the bilirubin level in the bile, which could facilitate the formation of gallstones because bilirubin is also a component of such stones. This hypothesis is supported by a case report that showed the presence of indinavir, another protease inhibitor, in the gallstones of a patient on indinavir-containing ART.[18] Indinavir has similar characteristics to atazanavir: optimal solubility at low pH and being an inhibitor of UGT1A1.[18,19]

There are several limitations to our study. First, because stone composition analysis was not conducted in this study, one cannot rule out other causes of cholelithiasis in addition to atazanavir/ritonavir. Second, the prevalence of gallstones is generally lower in Asians than in Europeans and since most of the patients in this study were Asian, the effect of atazanavir/ritonavir might be different in other populations.[20] Third, because the study population included patients who had undergone abdominal ultrasonography in clinical practice with various indications, the prevalence of cholelithiasis might be overestimated.

In conclusion, the present study demonstrated that patients on long-term treatment (>2 years) with atazanavir/ritonavir were twice as likely to develop cholelithiasis compared with those treated for <2 years. A similar effect was not demonstrated in patients treated with lopinavir/ritonavir or darunavir/ritonavir. Long-term, large prospective studies are warranted to elucidate the incidence and risk factors for complicated cholelithiasis in patients exposed to atazanavir/ritonavir-containing ART.

## Acknowledgements

We thank Motoshi Maejima, a senior staff member at the Physiological Examination Unit, and Mikiko Ogata and Michiyo Ishisaka for their invaluable contribution to the study. We also thank Akiko Nakano for supporting this study as a research coordinator and all the clinical staff at the AIDS Clinical Center for their help in the completion of this study.

## Funding

This work was supported by Grants-in Aid for AIDS research from the Japanese Ministry of Health, Labour, and Welfare (H23-AIDS-001).

## Transparency declarations

H. G. has received honoraria from MSD K.K., Abbott Japan, Co., Janssen Pharmaceutical K.K., Torii Pharmaceutical, Co. and ViiV Healthcare, Co. S. O. has received honoraria and research grants from MSD K.K., Abbott Japan, Co., Janssen Pharmaceutical K.K., Pfizer, Co. and Roche Diagnostics K.K., and has received honoraria from Astellas Pharmaceutical K.K., Bristol-Myers K.K., Daiichisankyo, Co., Dainippon Sumitomo Pharma, Co., GlaxoSmithKline K.K., Taisho Toyama Pharmaceutical, Co., Torii Pharmaceutical, Co. and ViiV Healthcare. All other authors: none to declare.

## Supplementary data

Figure S1 is available as Supplementary data at *JAC* Online (http://jac.oxfordjournals.org/).

## References

**1** Squires K, Lazzarin A, Gatell JM *et al.* Comparison of once-daily atazanavir with efavirenz, each in combination with fixed-dose zidovudine and lamivudine, as initial therapy for patients infected with HIV. *J Acquir Immune Defic Syndr* 2004; **36**: 1011–9.

**2** Molina JM, Andrade-Villanueva J, Echevarria J *et al.* Once-daily atazanavir/ritonavir compared with twice-daily lopinavir/ritonavir, each in combination with tenofovir and emtricitabine, for management of antiretroviral-naive HIV-1-infected patients: 96-week efficacy and safety results of the CASTLE study. *J Acquir Immune Defic Syndr* 2010; **53**: 323–32.

**3** Panel on Antiretroviral Guidelines for Adults and Adolescents. *Guidelines for the Use of Antiretroviral Agents in HIV-1-Infected Adults and Adolescents*. Department of Health and Human Services. http://www.aidsinfo.nih.gov/ContentFiles/AdultandAdolescentGL.pdf (25 November 2013, date last accessed).

**4** *Reyataz (Atazanavir Sulfate): Full Prescription Information (Package Insert)*. Princeton: Bristol-Myers Squibb, 2012.

**5** Rakotondravelo S, Poinsignon Y, Borsa-Lebas F *et al.* Complicated atazanavir-associated cholelithiasis: a report of 14 cases. *Clin Infect Dis* 2012; **55**: 1270–2.

**6** Courbon E, Laylavoix F, Soulie C *et al.* Unexpected atazanavir-associated biliary lithiasis in an HIV-infected patient. *J Antimicrob Chemother* 2012; **67**: 250–1.

**7** Jacques AC, Giguere P, Zhang G *et al.* Atazanavir-associated choledocholithiasis leading to acute hepatitis in an HIV-infected adult. *Ann Pharmacother* 2010; **44**: 202–6.

**8** Hamada Y, Nishijima T, Komatsu H *et al.* Is ritonavir-boosted atazanavir a risk for cholelithiasis compared to other protease inhibitors? *PLoS One* 2013; **8**: e69845.

**9** Barbara L, Sama C, Morselli Labate AM *et al.* A population study on the prevalence of gallstone disease: the Sirmione Study. *Hepatology* 1987; **7**: 913–7.

**10** Nishijima T, Komatsu H, Higasa K *et al.* Single nucleotide polymorphisms in ABCC2 associate with tenofovir-induced kidney tubular dysfunction in Japanese patients with HIV-1 infection: a pharmacogenetic study. *Clin Infect Dis* 2012; **55**: 1558–67.

**11** The epidemiology of gallstone disease in Rome, Italy. Part II. Factors associated with the disease. The Rome Group for Epidemiology and Prevention of Cholelithiasis (GREPCO). *Hepatology* 1988; **8**: 907–13.

**12** Conte D, Fraquelli M, Fornari F *et al.* Close relation between cirrhosis and gallstones: cross-sectional and longitudinal survey. *Arch Intern Med* 1999; **159**: 49–52.

**13** De Santis A, Attili AF, Ginanni Corradini S *et al.* Gallstones and diabetes: a case–control study in a free-living population sample. *Hepatology* 1997; **25**: 787–90.

**14** Hamada Y, Nishijima T, Watanabe K *et al.* High incidence of renal stones among HIV-infected patients on ritonavir-boosted atazanavir than in those receiving other protease inhibitor-containing antiretroviral therapy. *Clin Infect Dis* 2012; **55**: 1262–9.

**15** Rockwood N, Mandalia S, Bower M *et al.* Ritonavir-boosted atazanavir exposure is associated with an increased rate of renal stones compared with efavirenz, ritonavir-boosted lopinavir and ritonavir-boosted darunavir. *AIDS* 2011; **25**: 1671–3.

**16** Le MP, Stitou H, Soulie C *et al.* Sialolithiasis in an HIV-1-infected patient treated with atazanavir/ritonavir monotherapy. *J Antimicrob Chemother* 2013; **68**: 727–9.

**17** Zhang D, Chando TJ, Everett DW *et al.* In vitro inhibition of UDP glucuronosyltransferases by atazanavir and other HIV protease inhibitors

and the relationship of this property to in vivo bilirubin glucuronidation. *Drug Metab Dispos* 2005; **33**: 1729–39.

**18** Verdon R, Daudon M, Albessard F *et al.* Indinavir-induced cholelithiasis in a patient infected with human immunodeficiency virus. *Clin Infect Dis* 2002; **35**: e57–9.

**19** Siveke JT, Bogner JR. Cholelithiasis possibly induced by protease inhibitors in 3 patients. *Clin Infect Dis* 2003; **36**: 1498–500.

**20** Shaffer EA. Epidemiology and risk factors for gallstone disease: has the paradigm changed in the 21st century? *Curr Gastroenterol Rep* 2005; **7**: 132–40.

AIDS RESEARCH AND HUMAN RETROVIRUSES
Volume 30, Number 6, 2014

DOI: 10.1089/aid.2013.0252



# Long-Term Use of Protease Inhibitors Is Associated with Bone Mineral Density Loss

Ei Kinai, Takeshi Nishijima, Daisuke Mizushima, Koji Watanabe, Takahiro Aoki, Haruhito Honda, Hirohisa Yazaki, Ikumi Genka, Junko Tanuma, Katsuji Teruya, Kunihisa Tsukada, Hiroyuki Gatanaga, Yoshimi Kikuchi, and Shinichi Oka

## Abstract

HIV-infected patients are at high risk for bone mineral density (BMD) loss. The present study was designed to provide information on characteristics of BMD abnormalities in Japanese HIV-1-infected patients and risk factors involved in worsening of BMD. A total of 184 Japanese HIV-1-infected men were studied with a dual-energy X-ray absorptiometry scan (DXA) at the lumbar spine and femoral neck. Multivariate logistic regression models were used for comparison of the impact of risk factors on BMD loss. Osteopenia and osteoporosis were diagnosed in 46% and 10% of the patients at lumbar spine, and 54% and 12% at femoral neck, respectively. In logistic analysis, factors associated with low BMD at both lumbar spine and femoral neck were long-term treatment with a protease inhibitor (PI) [odds ratio (OR) 1.100 and 1.187 per 1 year increase of PI use; 95% confidence interval (CI) 1.003–1.207 and 1.043–1.351; $p=0.042$ and 0.009, respectively] and a low body mass index [OR: 0.938 and 0.852, CI 0.892–0.992 and 0.783–0.927; $p=0.024$ and $<0.001$, respectively]. Patients who discontinued PI had a significantly higher BMD than those who currently use PI at lumbar spine ($t$ score $-0.8$ vs. $-1.3$, $p=0.04$) but not at femoral neck ($-1.3$ vs. $-1.5$, $p=0.38$). In HIV-infected Japanese patients, the duration of treatment with PI correlated significantly with BMD loss. Discontinuation of PI is a promising option in the treatment of BMD loss since it allows recovery of BMD, especially in the lumbar spine.

## Introduction

For HIV-infected patients, loss of bone mineral density (BMD) is an important age-related complication, in addition to chronic renal dysfunction, cardiovascular diseases, and metabolic disorders. A meta-analysis study reported that the prevalence of osteoporosis among HIV-infected patients was three times higher than in the HIV-negative population.[1] The etiology of low BMD in HIV-infected patients is multifactorial and is considered to include chronic HIV infection[2,3] and antiretroviral therapy, especially tenofovir disoproxil fumarate (TDF) and protease inhibitors (PI).[4–7] However, to our knowledge, information on the characteristics of BMD abnormalities in Asian HIV-infected patients is scarce and the exact risk factors involved in the worsening of BMD remain obscure. The present study was designed to provide new information on the above two aspects of Asian HIV-1 infection.

## Materials and Methods

### *Setting and participants*

We performed a cross-sectional study at the AIDS Clinical Center (ACC), National Center for Global Health and Medicine (NCGM) involving HIV-infected patients who were registered at the NCGM from February 2012 to June 2013. We excluded patients who had been on treatment for osteoporosis, current users of corticosteroids, and those with a history of bone fractures at the spine or bilateral femoral neck. A total of 184 Japanese HIV-infected men were enrolled in this study. This study was approved by the ethics committee of NCGM and a written informed consent was obtained from each patient.

### *Data collection*

BMD was assessed using dual X-ray absorptiometry (DXA: QDR-4500W, Hologic Inc., Bedford, MA) at the lumbar spine

AIDS Clinical Center, National Center for Global Health and Medicine, Tokyo, Japan.

and femoral neck. Osteopenia and osteoporosis were defined using the World Health Organization (WHO) criteria. Normal BMD was defined as a $t$ score of $-1$ or higher, osteopenia as a $t$ score between $-1$ and $-2.5$, and osteoporosis as a $t$ score of $-2.5$ or lower.[8] Age, body mass index (BMI), smoking habit, hemophilia, history of an AIDS-defined illness, nadir CD4 cell count, time with low CD4 cell count (<200 cell/$\mu$l), time on antiretroviral therapy (ART), TDF, and PI, were obtained by interview or medical records. Estimated glomerular filtration rate (eGFR) was calculated using the modified Modification of Diet in Renal Disease (MDRD) equation for Japanese populations.[9]

### *Statistical analysis*

$t$ scores and BMD of the lumbar spine and femoral neck were compared using Student's paired $t$-test. To determine the impact of independent variables, multivariate logistic regression analysis was used. In logistic regression analysis, the dependent variable was set as low BMD ($t$ score lower than $-1.0$) at both the lumbar spine and femoral neck. We used the odds ratio (ORs) and 95% confidence interval (95% CI) to estimate the impact of each variable on low BMD.

To assess the impact of PI discontinuation, we compared the $t$ scores between PI-experienced patients and patients who discontinued such therapy, using the Student's unpaired $t$-test. For evaluation of the correlation between the $t$ score at the lumbar spine and the time on PI, ritonavir (RTV) at different dosage (100 mg/day and 200 mg/day), and other types of PI, Pearson's correlation coefficient was used. For further evaluation of the relationship between the time on TDF and BMD, we compared the $t$ scores between those who were treated with PI plus TDF and those treated with PI only and had never been treated with TDF, using the Student's unpaired $t$-test. All statistical analyses were performed with The Statistical Package for Social Sciences ver. 17.0 (SPSS, Chicago, IL).

## Results

### *Patient characteristics*

The characteristics of the 184 study patients are summarized in Table 1. All patients underwent DXA for the lumbar spine and 164 underwent DXA for the femoral neck. Hemophiliacs constituted 36% ($n=67$) of the study subjects. Seventy-one patients (39%) had a history of infection with hepatitis C virus (HCV), including all 67 hemophiliacs. Among them, 16 of the 71 (23%) patients showed spontaneous viral clearance, 23 (32%) achieved sustained virologic response after antiviral therapy, and 2 (3%) patients were still on treatment and had undetectable levels of HCV viral load. The remaining 30 (45%) patients with chronic hepatitis C were nonresponders or never users of antiviral therapy. Among them, 9 (14%) had liver cirrhosis diagnosed by radiological findings. Although 41 (21%) patients had a history of AIDS-defined illness, 172 (93%) patients had been treated with ART and 148 (80%) patients had an undetectable level of HIV viral load.

The median durations of ART, PI, and TDF of the total population were 88, 38, and 23 months, respectively. Among 139 TDF-treated patients, the median time on TDF was 38 months (IQR 14–68 months). One hundred and forty-four patients had previously received PI-based treatment, and the numbers of patients who had been treated with each type of PI were 30 patients with nelfinavir (NFV), 47 with lopinavir (LPV/r), 34 with atazanavir (ATV), 21 with fosamprenavir (FPV) or amprenavir (APV), 74 with darunavir (DRV), 4 with indinavir (IDV), and 1 with saquinavir (SQV). The total number of patients who had received RTV was 137, and of these, 102 and 63 patients had been treated with RTV at 100 and 200 mg/day, respectively.

Table 1. Clinicopathological Characteristics of the 184 Study Patients

| | |
|---|---|
| Sex, (male/female) | 184/0 |
| Age: median (IQR) | 43 (38–51) |
| Body mass index (kg/m$^2$) | 22 (20–24) |
| Hypertension, $n$ (%) | 42 (23%) |
| Current smoking, $n$ (%) | 99 (54%) |
| Hemophilia, $n$ (%) | 67 (36%) |
| History of AIDS-defined illness, $n$ (%) | 40 (22%) |
| Positive HBsAg, $n$ (%) | 8 (4%) |
| Positive HCV-Ab, $n$ (%) | 71 (37%) |
| Liver cirrhosis, $n$ (%) | 10 (5%) |
| Diabetes mellitus, $n$ (%) | 7 (4%) |
| Current CD4$^+$ T cell count (cells/$\mu$l) | 493 (322–623) |
| Nadir CD4$^+$ T cell count (cells/$\mu$l) | 141 (54–218) |
| Low CD4$^+$ T cell count (<200 cells/$\mu$l) for >1 year, $n$ (%) | 52 (28%) |
| Current suppressed viral load (<20 copies/ml), $n$ (%) | 148 (80%) |
| Current use of ART, $n$ (%) | 172 (93%) |
| Time on ART (months) | 88 (26–153) |
| Current use of protease inhibitors, $n$ (%) | 117 (64%) |
| Never use of protease inhibitors, $n$ (%) | 40 (22%) |
| Time on protease inhibitors (months) | 38 (2–81) |
| Current use of tenofovir, $n$ (%) | 114 (62%) |
| Never use of tenofovir, $n$ (%) | 45 (24%) |
| Time on tenofovir (months) | 22 (0–60) |
| Serum creatinine (mg/dl) | 0.78 (0.68–0.89) |
| Estimated glomerular filtration rate (ml/min/1.73 m$^2$) | 86.0 (74.7–100.3) |

Values are median (IQR) or number (%) of patients.
HBsAg, hepatitis B virus surface antigen; HCV-Ab, hepatitis C virus antibody; ART, antiretroviral therapy; ART, antiretroviral therapy.

### *Prevalence of low bone mineral density*

Based on the WHO criteria, osteopenia and osteoporosis were diagnosed in 46% and 10% of the patients at the lumbar spine and 53% and 12% at the femoral neck, respectively. The mean $t$ scores were $-1.1$ [standard deviation (SD) 1.1] for the lumbar spine and $-1.4$ (SD: 1.1) for the femoral neck (Fig. 1A). The mean BMD scores were 0.914 g/cm$^2$ (SD: 0.199 g/cm$^2$) at the lumbar spine and 0.694 g/cm$^2$ (SD: 0.221 g/cm$^2$) at the femoral neck (Fig. 1B). Both the $t$ score and BMD at the femoral neck were significantly lower than those at the lumbar spine ($p=0.008$ for $t$ score and $p<0.001$ for BMD).

### *Impact of related risk factors*

In multivariate logistic analysis, statistically significant regression models were built for low BMD ($t$ score $<-1$) at the lumbar spine ($p=0.038$) and at the femoral neck

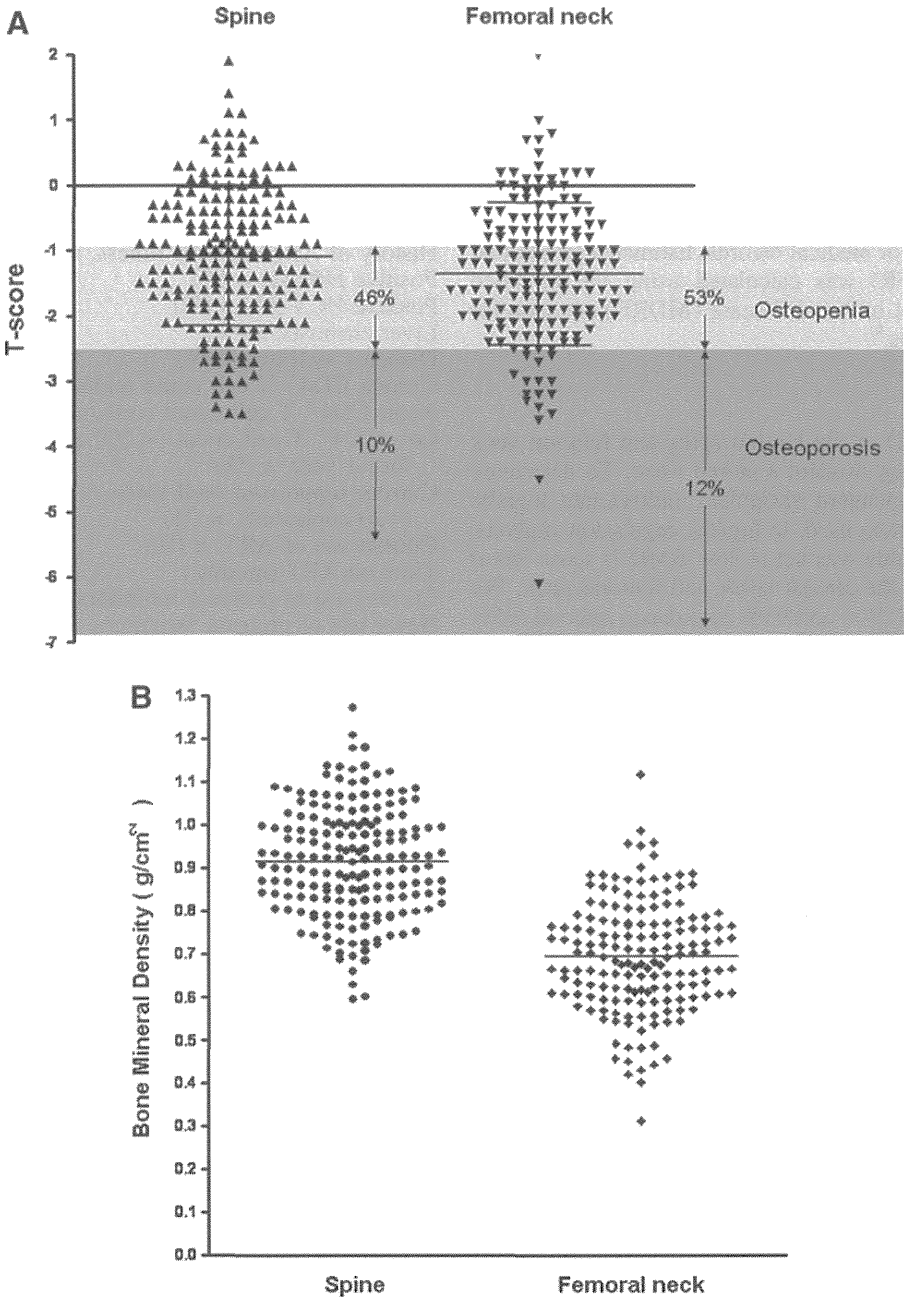


**FIG. 1.** **(A)** Distribution of *t* scores at lumbar spine and femoral neck. Light areas: osteopenia; dark gray areas: osteoporosis. **(B)** Distribution of bone mineral density (BMD) at lumbar spine and femoral neck. In both **(A)** and **(B)**, data are mean ± standard deviation. Differences in the mean scores of the spine and femoral neck were tested by the Student's paired *t*-test.

($p < 0.001$) (Table 2). In logistic analysis, the following factors were associated with low BMD at both the lumbar spine and femoral neck: longer duration of treatment with a PI [odds ratio (OR) 1.100 and 1.187 per 1 year increase of PI use and 95% confidence interval (CI) 1.003–1.207 and 1.043–1.351; $p = 0.042$ and 0.009, respectively] and lower body mass index [OR: 0.938 and 0.852, CI 0.892–0.992 and 0.783–0.927; $p = 0.024$ and $< 0.001$, respectively]. Low BMD at the femoral neck also correlated with age [OR: 1.071; CI 1.029–1.115; $p = 0.001$] and hemophilia [OR: 8.139; CI 2.594–25.337; $p < 0.001$].

*Impact of PI use and discontinuation on bone mineral density*

The *t* scores of both the spine and femoral neck were significantly lower in patients who received PI than in those who never used PI [−1.2 vs. −0.7 at the spine ($p = 0.02$) and −1.5 vs. −0.9 at the femoral neck ($p = 0.002$), respectively] (Fig. 2A). Moreover, patients who discontinued PI had a higher spine *t* score than those who currently used PI (−0.8 vs. −1.3, $p = 0.04$) and had a *t* score level comparable to those patients who never used PI (−0.8 in PI-discontinued patients

TABLE 2. RESULTS OF LOGISTIC ANALYSIS FOR BONE MINERAL ABNORMALITIES MEASURED FOR DIFFERENT JOINTS

| | *Univariate analysis* | | | *Multivariate analysis*[a] | | |
|---|---|---|---|---|---|---|
| | *OR* | *95% CI* | p *value* | *OR* | *95% CI* | p *value* |
| Low BMD at lumbar spine ($t$ score $< -1.0$) | | | | | | |
| Age (per 1 year increase) | 1.015 | 0.986–1.045 | 0.309 | 1.016 | 0.989–1.042 | 0.249 |
| Body mass index (per 1 increase) | 0.924 | 0.845–1.011 | 0.086 | 0.938 | 0.892–0.992 | 0.024 |
| Hemophilia | 1.013 | 0.556–1.847 | 0.967 | | | |
| Current smoking | 1.690 | 0.942–3.302 | 0.078 | 1.651 | 0.903–2.971 | 0.104 |
| History of AIDS-defined illness | 1.630 | 0.800–3.323 | 0.176 | | | |
| Nadir CD4 (per 1 increase of categories) | | | | | | |
| ≥350 | 1.000 | | | | | |
| 200–349 | 0.514 | 0.140–1.883 | 0.315 | | | |
| ≤199 | 0.799 | 0.241–2.653 | 0.714 | | | |
| Time with CD4 <200/μl (per 1 year increase) | 1.065 | 0.921–1.233 | 0.515 | | | |
| Time on ART (per 1 year increase) | 1.027 | 0.978–1.077 | 0.287 | 0.973 | 0.912–1.038 | 0.408 |
| Time on TDF (per 1 year increase) | 1.082 | 0.976–1.200 | 0.134 | 1.078 | 0.961–1.210 | 0.201 |
| Time on PI (per 1 year increase) | 1.081 | 1.009–1.159 | 0.026 | 1.100 | 1.003–1.207 | 0.042 |
| Low BMD at femoral neck ($t$-score $< -1.0$) | | | | | | |
| Age (per 1 year increase) | 1.012 | 1.005–1.019 | 0.001 | 1.071 | 1.029–1.115 | 0.001 |
| Body mass index (per 1 increase) | 1.017 | 1.003–1.031 | 0.018 | 0.852 | 0.783–0.927 | <0.001 |
| Hemophilia | 3.954 | 1.850–8.448 | <0.001 | 8.139 | 2.594–25.337 | <0.001 |
| Current smoking | 1.206 | 0.642–2.265 | 0.561 | 0.238 | 0.734–3.460 | 0.238 |
| History of AIDS-defined illness | 1.870 | 0.806–4.338 | 0.141 | 0.124 | 0.795–6.789 | 0.124 |
| Nadir CD4 (per 1 increase of categories) | | | | | | |
| ≥350 | 1.000 | | | 1.000 | | |
| 200–349 | 1.593 | 0.425–5.971 | 0.489 | 1.553 | 0.355–6.783 | 0.559 |
| ≤199 | 0.984 | 0.293–3.301 | 0.979 | 0.757 | 0.174–3.285 | 0.710 |
| Time with CD4 <200/μl (per 1 increase of categories) | 1.072 | 0.951–1.209 | 0.257 | 0.844 | 0.684–1.042 | 0.114 |
| Time on ART (per 1 year increase) | 1.070 | 1.034–1.117 | <0.001 | 0.968 | 0.880–1.066 | 0.509 |
| Time on TDF (per 1 year increase) | 1.084 | 1.005–1.119 | 0.037 | 0.990 | 0.848–1.156 | 0.900 |
| Time on PI (per 1 year increase) | 1.151 | 1.079–1.225 | <0.001 | 1.187 | 1.043–1.351 | 0.009 |

[a]In the analysis for lumbar spine, the final model obtained by backward stepwise elimination included the time on ART, TDF, and PI, current smoking, BMI, and age. OR, odds ratios; CI, confidence intervals; ART, antiretroviral therapy; TDF, tenofovir disoproxil fumarate; PI, protease inhibitors; BMD, bone mineral density.

vs. −0.7 in PI-never use patients, $p=0.97$) (Fig. 2B). In contrast, there was no significant difference in femoral neck $t$ score between PI-discontinued patients and PI current-use patients (−1.3 vs. −1.5, $p=0.38$) or between PI-discontinued patients and PI-never use patients (−1.3 vs. −0.9, $p=0.24$) (Fig. 2C).

### *Impact of different types of PIs on bone mineral density*

While the correlation between the duration of treatment of any PI and spine $t$ score was significant ($r=-0.180$, $p=0.013$) (Fig. 3A), the duration of treatment with RTV showed a better correlation with spine $t$ score ($-0.207$, $p=0.004$) (Fig. 3B). When both the time on RTV and the time on PI were entered as independent variables in logistic analysis for low BMD at the lumbar spine, a statistically significant model was built by elimination of the time on PI. In this model, the time on RTV was significantly associated with low BMD (OR: 1.146, 95% CI 1.032–1.273, $p=0.011$). At the femoral neck, RTV was associated with low BMD (OR: 1.267 per 1 year increase of RTV, 95% CI 1.010–1.589, $p=0.041$), whereas the time on PI was not (OR: 0.983 per 1 year increase of PI, 95% CI 0.803–1.202, $p=0.864$). There were no significant correlations between spine $t$ score and the duration of treatment with RTV at either 100 mg/day ($r=-0.134$, $p=0.071$) (Fig. 3C) or 200 mg/day ($r=-0.133$, $p=0.073$) (Fig. 3D). No significant correlations were found between different types of PIs and spine $t$ score (NFV: $r=-0.023$, $p=0.758$; LPV/r: $r=-0.080$, $p=0.239$; DRV: $r=-0.069$, $p=0.355$; ATV: $r=-1.123$, $p=0.097$; FPV or APV: $r=0.091$, $p=0.218$).

### *Comparison of BMD between PI- and PI-TDF-treated patients*

For further confirmation of the poor association between TDF use and BMD loss, $t$ scores were compared between patients who had been treated with both PI and TDF ($n=118$) and patients who received PI-based treatment and had never been treated with TDF ($n=26$). Neither spine nor femoral neck $t$ scores were significantly different between the two groups (PI + TDF: −1.2, PI alone: −1.0, $p=0.414$ for spine $t$ score, −1.5 vs. −1.5, $p=0.844$ for femoral neck, respectively).

## Discussion

The present study showed that for Asian HIV-infected patients, PI use was the most significant determinant of low BMD at both the spine and femoral neck. Moreover, our logistic regression models strongly suggested that long-term use of PI has a gradual and cumulative effect on BMD.

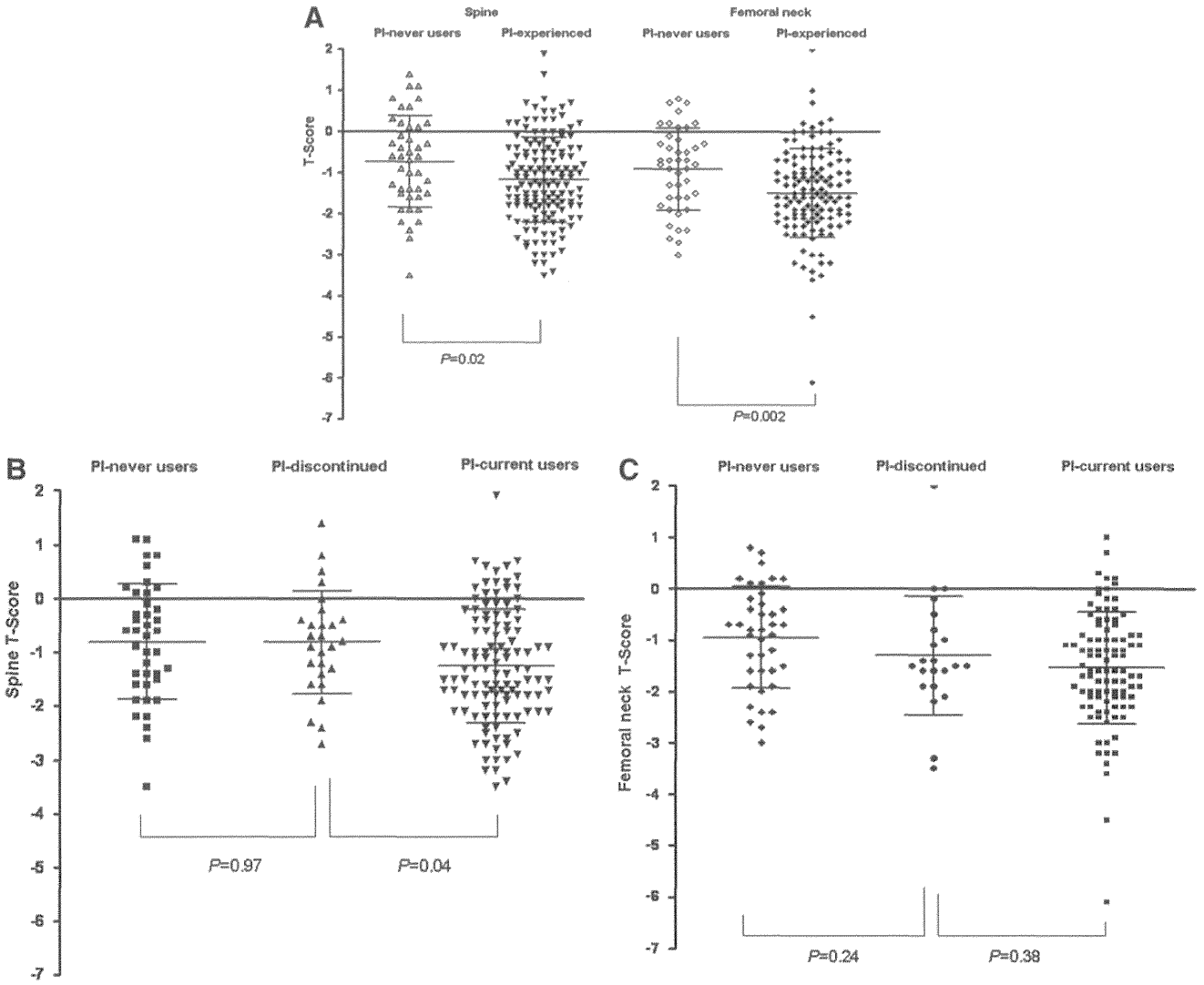


**FIG. 2.** (**A**) Comparison of *t* scores at lumbar spine and femoral neck between patients who were treated and never treated with a protease inhibitor (PI). Comparison of *t* score at lumbar spine (**B**) and at femoral neck (**C**) among patients who never used PI (left), discontinued PI (center), and are currently using PI (right). Data are mean ± standard deviation.

Although large cohort studies have already shown that PI use can cause BMD loss,[4–6] it still remains unclear which type of PI causes BMD loss. Our study found no significant association between the use of any particular type of PI and BMD loss, which is consistent with a previous *in vitro* study that evaluated the impact of different PIs on osteoblast activity using an osteoblast-like cell line.[10] Both *in vitro*[11,12] and *ex vivo* studies[13] reported that RTV promotes the proliferation/activation of osteoclasts, causing increased bone absorption. Our study added support to previous studies that RTV plays a major role in PI-associated BMD loss,[13] although there is insufficient data to conduct direct a comparison of BMD between patients treated with unboosted and boosted PI. The correlations between the two different dosages of RTV and BMD were almost comparable levels of strength, suggesting that RTV can cause BMD loss not dose dependently but time dependently irrespective of the dose. However, at this stage, we recommend further evaluation of the effect of each type of PI, since the subanalyses conducted in the present study have limited power for cause–effect evaluation due to the relatively small number of patients treated with certain types of PI.

Does discontinuation of PI lead to recovery of BMD? It seems there is no definitive answer to this question. A small cohort substudy showed possible BMD recovery after switching PI to raltegravir.[14] However, the change in BMD after switching was too small in that study to confirm the recovery effect of PI discontinuation. The present study provides additional data in support of a lower decrease in BMD by showing a large difference in BMD between PI-discontinued and -continued patients, although it is a cross-sectional study. A prospective longitudinal cohort study using a larger population on longer use of PI is necessary for a more precise evaluation of the reversibility of PI-associated BMD loss. It should be noted that the PI-discontinued patients showed a higher BMD level not in the femoral neck but in the lumbar spine, which is consistent with some large cohort study showing that PI causes greater BMD loss in the lumbar spine than the femoral neck.[4,5] This interesting discrepancy is well explained by the difference in bone tissue

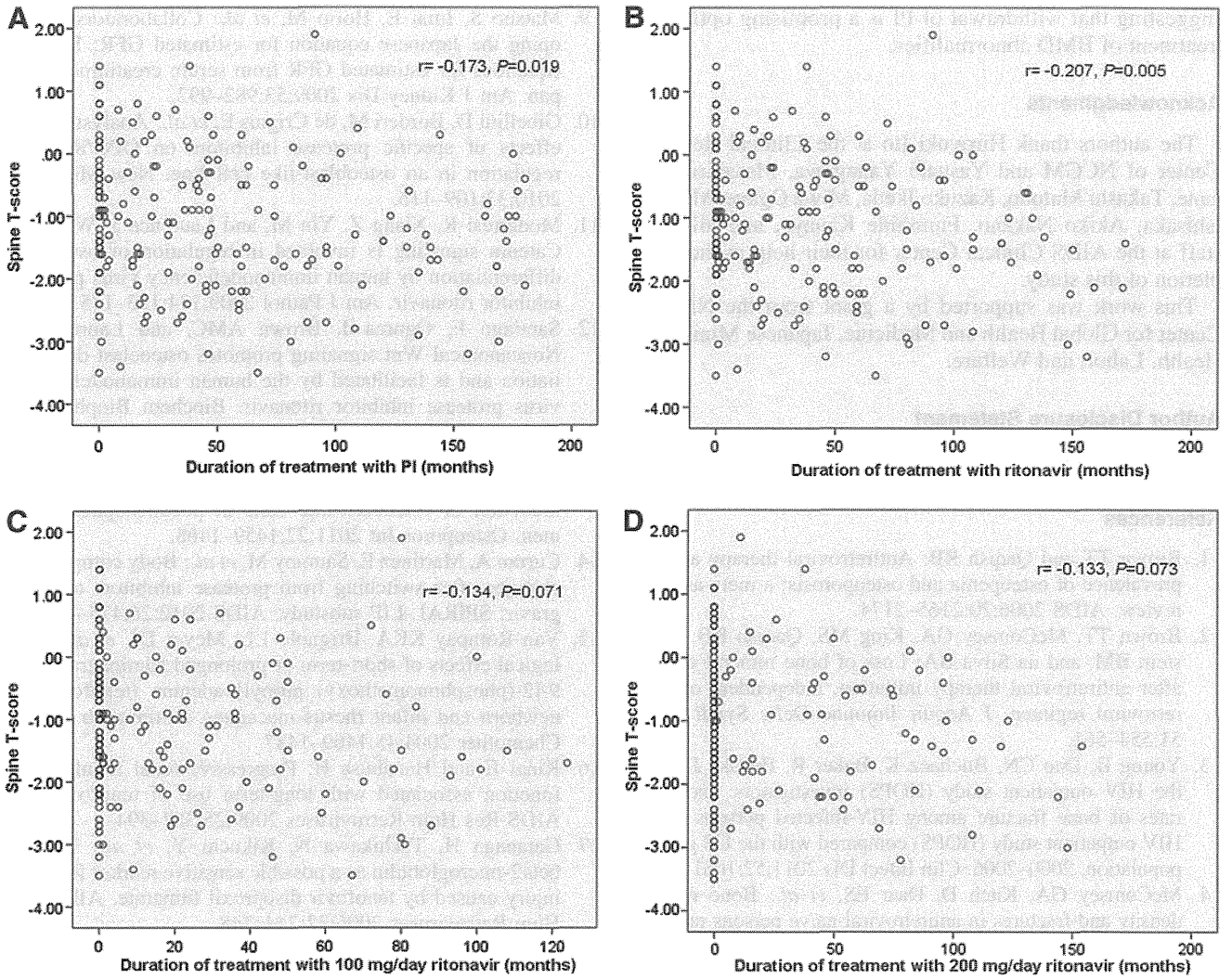


**FIG. 3.** Scattered dot plots of the correlation between *t* score at lumbar spine and duration of treatment with PI **(A)**, ritonavir (RTV) **(B)**, RTV at 100 mg/day **(C)**, and RTV at 200 mg/day **(D)**. Correlations were tested by Pearson's correlation coefficient.

type between the vertebrae and femur. While the femur contains abundant cortical substance with few osteoclasts, the vertebrae comprise osteoclast-rich trabecular substance. Therefore, discontinuation of osteoclast-activating agents, such as RTV, can cause a slower decrease of BMD in vertebrae compared with the femur.

TDF can cause BMD loss mainly through persistent urinary loss of phosphates.[4,7,15,16] However, our study did not show any significant association between TDF use and low BMD. While the exact reason for this finding is not clear, it could be related to the general clinical practice in Japan: TDF is often discontinued in Japan upon identification of modest proximal tubular dysfunction (a low level of percent tubular reabsorption of phosphates or a high level of urine-$\beta_2$-microglobulin) in HIV-infected patients.[16,17] This practice is an important limitation in the present study.

Hemophilia is a risk factor for BMD loss based on the associated hemophilic arthropathy and long-term disuse.[18,19] However, the present study demonstrated an almost equal prevalence of spine BMD abnormalities in hemophiliacs and HIV-infected patients [rate of osteoporosis, hemophiliacs: 5/67 (7%), other patients: 14/117 (12%); rate of osteopenia, hemophiliacs: 32/67 (48%), other patients: 52/117 (44%)]. Furthermore, the mean (standard deviation) *t* score of the lumbar spine was −1.1 (1.0) in hemophiliacs and −1.1 (1.1) in other patients. Thus, with regard to lumbar spine BMD, the present study well reflects the general Asian HIV-infected population. On the other hand, BMD abnormalities are common in hemophiliacs including abnormalities of the femoral neck [rate of osteoporosis, hemophiliacs: 15/57 (26%), other patients: 5/107 (5%); rate of osteopenia, hemophiliacs: 32/57 (56%), other patients: 56/107 (52%)]. The mean (standard deviation) *t* score of the femoral neck was −2.0 (1.1) in hemophiliacs and −1.0 (0.9) in other patients. Multivariate analysis identified age, BMI, and hemophilia as significant determinants of BMD at the femoral neck. Thus, BMD at the femoral neck is considered to be largely influenced by weight load and disuse.

In conclusion, long-term use of PI was identified as a significant risk factor for BMD loss in HIV-infected Asian patients. Furthermore, the results demonstrated that the negative effect of PI on BMD was time dependent. In particular, RTV plays a major role in PI-associated BMD loss irrespective of the dose. Discontinuation of PI seems to lessen the decrease in BMD, especially in the lumbar spine,

suggesting that withdrawal of PI is a promising option for treatment of BMD abnormalities.

### Acknowledgments

The authors thank Hiroyuki Ito at the Clinical Research Center of NCGM and Yasuaki Yanagawa, Masahiro Ishikane, Takashi Matono, Kazuko Ikeda, Miwa Ogane, Michiyo Ishisaka, Akiko Nakano, Fumihide Kanaya, and all other staff at the AIDS Clinical Center for their help in the completion of this study.

This work was supported by a grant from the National Center for Global Health and Medicine, Japanese Ministry of Health, Labor, and Welfare.

### Author Disclosure Statement

No competing financial interests exist.

### References

1. Brown TT and Qaqish RB: Antiretroviral therapy and the prevalence of osteopenia and osteoporosis; a meta-analytic review. AIDS 2006;20:2165–2174.
2. Brown TT, McComsey GA, King MS, Qaqish RB, Bernstein BM, and da Silva BA: Loss of bone mineral density after antiretroviral therapy initiation, independent of antiretroviral regimen. J Acquir Immune Defic Syndr 2009; 51:554–561.
3. Young B, Dao CN, Buchacz K, Baker R, Brooks JT, and the HIV outpatient study (HOPS) investigators: Increased rates of bone fracture among HIV-infected persons in the HIV outpatient study (HOPS) compared with the US general population, 2000–2006. Clin Infect Dis 2011;52:1061–1068.
4. McComsey GA, Kitch D, Daar ES, *et al.:* Bone mineral density and fractures in antiretroviral-naïve persons randomized to receive abacavir-lamivudine or tenofovir disoproxil fumarate-emtricitabine along with efavirenz or atazanavir-ritonavir: AIDS clinical trials group A5224s, a substudy of ACTG A5202. J Infect Dis 2011;203:1791–1801.
5. Duvivier C, Kolta S, Assoumou L, *et al.:* Greater decrease in bone mineral density with protease inhibitor regimens compared with non-nucleoside reverse transcriptase inhibitor regimens in HIV-1 infected naive patients. AIDS 2009; 23:817–824.
6. Bonjoch A, Figueras M, Estany C, *et al.:* High prevalence of and progression to low bone mineral density in HIV-infected patients: A longitudinal cohort study. AIDS 2010; 24:2827–2833.
7. Moyle GJ, Stellbrink HJ, Compston J, *et al.:* 96-week results of abacavir/lamivudine versus tenofovir/emtricitabine, plus efavirenz, in antiretroviral-naïve, HIV-1-infected adults: ASSERT study. Antivir Ther 2013;18:905–913.
8. Prevention and management of osteoporosis. World Health Organ Tech Rep Ser 2003;921:1–164
9. Matsuo S, Imai E, Horio M, *et al.:* Collaborators developing the Japanese equation for estimated GFR: Revised equations for estimated GFR from serum creatinine in Japan. Am J Kidney Dis 2009;53:982–992.
10. Gibellini D, Borderi M, de Crignis E, *et al.:* Analysis of the effects of specific protease inhibitors on OPG/RANKL regulation in an osteoblast-like cell line. New Microbiol 2010;33:109–115.
11. Modarresi R, Xiang Z, Yin M, and Laurence J: WNT/ β-Catenin signaling is involved in regulation of osteoclast differentiation by human immunodeficiency virus protease inhibitor ritonavir. Am J Pathol 2009;174:123–135.
12. Santiago F, Oguma J, Brown AMC, and Laurence J: Noncanonical Wnt signaling promotes osteoclast differentiation and is facilitated by the human immunodeficiency virus protease inhibitor ritonavir. Biochem Biophys Res Commun 2012;417:223–230.
13. Yin, MT, Modaressi R, Shane E, *et al.:* Effects of HIV infection and antiretroviral therapy with ritonavir on induction of osteoclast-like cells in postmenopausal women. Osteoporos Int 2011;22:1459–1468.
14. Curran A, Martinez E, Saumoy M, *et al.:* Body composition changes after switching from protease inhibitors to raltegravir: SPIRAL-LIP substudy. AIDS 2012;26:475–481.
15. Van Rompay KKA, Brignolo LL, Meyer DJ, *et al.:* Biological effects of short-term or prolonged administration of 9-[2-(phosphonomethoxy) propyl] adenine (tenofovir) to newborn and infant rhesus macaques. Antimicrob Agents Chemother 2004;48:1469–1487.
16. Kinai E and Hanabusa H: Progressive renal tubular dysfunction associated with long-term use of tenofovir DF. AIDS Res Hum Retroviruses 2009;25:387–394.
17. Gatanaga H, Tachikawa N, Kikuchi Y, *et al.:* Urinary beta2-microglobulin as a possible sensitive marker for renal injury caused by tenofovir disoproxil fumarate. AIDS Res Hum Retroviruses 2006;22:744–748.
18. Gerstner G, Damiano ML, Tom A, *et al.:* Prevalence and risk factors associated with decreased bone mineral density in patients with haemophilia. Haemophilia 2009;15:559–565.
19. Nair AP, Jjina F, Ghosh K, Madkaikar M, Shrikhande M, and Nema M: Osteoporosis in young haemophiliacs from western India. Am J Hematol 2007;82:453–457.

Address correspondence to:
*Ei Kinai*
*AIDS Clinical Center*
*National Center for Global Health and Medicine, Tokyo*
*1-21-1, Toyama, Shinjuku-ku*
*Tokyo, 162-8655*
*Japan*

*E-mail:* ekinai@acc.ncgm.go.jp

# Molecular Basis of a Dominant T Cell Response to an HIV Reverse Transcriptase 8-mer Epitope Presented by the Protective Allele HLA-B*51:01

Chihiro Motozono,*,[1] Nozomi Kuse,†,[1] Xiaoming Sun,† Pierre J. Rizkallah,* Anna Fuller,* Shinichi Oka,†,‡ David K. Cole,*,[2] Andrew K. Sewell,*,[2] and Masafumi Takiguchi†,[2]

**CD8$^+$ CTL responses directed toward the HLA-B*51:01–restricted HIV-RT$_{128–135}$ epitope TAFTIPSI (TI8) are associated with long-term nonprogression to AIDS. Clonotypic analysis of responses to B51-TI8 revealed a public clonotype using TRAV17/TRBV7-3 TCR genes in six out of seven HLA-B*51:01$^+$ patients. Structural analysis of a TRAV17/TRBV7-3 TCR in complex with HLA–B51-TI8, to our knowledge the first human TCR complexed with an 8-mer peptide, explained this bias, as the unique combination of residues encoded by these genes was central to the interaction. The relatively featureless peptide-MHC (pMHC) was mainly recognized by the TCR CDR1 and CDR2 loops in an MHC-centric manner. A highly conserved residue Arg$^{97}$ in the CDR3α loop played a major role in recognition of peptide and MHC to form a stabilizing ball-and-socket interaction with the MHC and peptide, contributing to the selection of the public TCR clonotype. Surface plasmon resonance equilibrium binding analysis showed the low affinity of this public TCR is in accordance with the only other 8-mer interaction studied to date (murine 2C TCR–H-2K$^b$-dEV8). Like pMHC class II complexes, 8-mer peptides do not protrude out the MHC class I binding groove like those of longer peptides. The accumulated evidence suggests that weak affinity might be a common characteristic of TCR binding to featureless pMHC landscapes.** *The Journal of Immunology*, **2014, 192: 3428–3434.**

The cytotoxic payload delivered by CD8$^+$ CTLs destroys cells posing a threat to host health. To ensure that this cytotoxicity is specifically targeted toward aberrant cells, CTLs express a TCR that can distinguish between self- and non–self-peptides (usually ranging from 8–13 aa) presented on the surface of most nucleated cells in peptide–MHC class I (pMHCI) (1, 2). Thus, T cells have the ability to scan the cellular proteome via the cell surface, providing an important mechanism for targeting diseased cells. CTLs constitute our main defense against intracellular infections and can destroy virally infected cells. It is well established that certain HLA molecules, such as HLA-B*27, HLA-B*51, and HLA-B*57, are associated with better control of HIV infection (3–5). These findings attest to the importance of CD8$^+$ CTL responses in HIV infection and have generated considerable interest in the mechanisms behind this protection in HIV-1–infected individuals carrying these HLA alleles. In this study, we focused on the response to HLA-B*51:01–restricted HIV-RT$_{128–135}$ 8-mer epitope (TAFTIPSI [TI8]). HLA-B*51:01 is associated with slow progression to AIDS, and B51-TI8–specific T cells strongly suppress HIV-1 replication in vitro (6). Furthermore, the magnitude of the B51-TI8–specific CD8$^+$ T cell response was significantly correlated to low plasma viral load in chronically HIV-1–infected HLA-B*51:01$^+$ Japanese hemophiliacs, whereas no correlation was found between the magnitude of the CD8$^+$ T cell response to three other dominant HLA-B51–restricted HIV-1 epitopes (7). Collectively, these correlative data suggest that the response to B51-TI8–specific CD8$^+$ T cells might play an important role in the control of HIV-1 replication.

We undertook to dissect HLA-B*51:01–restricted CTL responses to this important epitope by examining the TCRs raised against the B51-TI8 epitope in responding patients. We identified a public CTL clone (3B) expressing a TCR encoded by TRAV17/TRBV7-3 TCR genes, specific for B51-TI8. We solved the structure of the 3B TCR in complex B51-TI8 and conducted a biophysical analysis of the interaction. To our knowledge, the 3B–B51-TI8 structure is the first human TCR complex with HLA-B*51:01 and the first containing a short 8-mer peptide without a prominent central bulge. Our data reveal the genetic and molecular mechanism explaining the predominance of TRAV17/TRBV7-3 TCRs in HLA-B*51:01$^+$ HIV$^+$ patients and provide new structural insights into CTL recognition of a flat 8-mer peptide presented by HLA-B*51:01.

*Cardiff University School of Medicine, Heath Park CF14 4XN, United Kingdom; †Center for AIDS Research, Kumamoto University, Chuo-ku, Kumamoto 860-0811, Japan; and ‡AIDS Clinical Center, National Center for Global Health and Medicine, Shinjuku-ku, Tokyo 162-8655, Japan

[1]C.M. and N.K. contributed equally to this work.

[2]D.K.C., A.K.S., and M.T. contributed equally to this work.

Received for publication October 2, 2013. Accepted for publication January 22, 2014.

This work was supported by the Global COE program "Global Education and Research Center Aiming at the Control of AIDS," launched as a project commissioned by the Ministry of Education, Science, Sports, and Culture, Japan, and the UK Biotechnology and Biological Sciences Research Council (Grant BB/H001085/1). D.K.C. is a Wellcome Trust Research Career Development Fellow (WT095767). P.J.R. was supported by a Research Council UK fellowship. This work was also supported in part by Grant GM067079 from the National Institute of General Medical Sciences, National Institutes of Health. A.K.S. is a Wellcome Trust Senior Investigator.

Address correspondence and reprint requests to Prof. Masafumi Takiguchi, Center for AIDS Research, Kumamoto University, 2-2-1 Honjo, Chuo-ku, Kumamoto 860-0811, Japan. E-mail address: masafumi@kumamoto-u.ac.jp

The online version of this article contains supplemental material.

Abbreviations used in this article: 7-AAD, 7-aminoactinomycin D; BSA, buried surface area; pMHC, peptide-MHC; pMHCI, peptide–MHC class I; pMHCII, peptide–MHC class II; SPR, surface plasmon resonance; TI8, TAFTIPSI; Vdw, Van der Waals.



www.jimmunol.org/cgi/doi/10.4049/jimmunol.1302667

## Materials and Methods

### *Patients*

Seven chronically HIV-1–infected Japanese individuals were recruited for the current study, which was approved by the ethics committees of Kumamoto University and the National Center for Global Health and Medicine, Japan. Written informed consent was obtained from all subjects according to the Declaration of Helsinki. We focused on seven HLA-B*51:01$^+$ Japanese individuals chronically infected with HIV-1 because HLA-B*51:01–restricted TI8-specific CTLs were induced by stimulating PBMCs from only these individuals with TI8 peptides. Three individuals (KI-021, KI-051, and KI-124) are hemophiliacs and long-term nonprogressors. Clinical records and HLA type of these individuals are shown in Supplemental Table I.

### *Generation of TI8-specific CTLs*

HLA-B*51:01–restricted TI8-specific CTL clones were generated from HIV-1–specific bulk-cultured T cells established from seven HLA-B*51:01$^+$ Japanese individuals chronically infected with HIV-1 by limiting dilution in U-bottom 96-well microtiter plates (Nunc, Roskilde, Denmark). Each well contained 200 μl cloning mixture (~$1 \times 10^6$ irradiated allogeneic PBMCs from healthy donors and $1 \times 10^5$ irradiated C1R-B*51:01 cells prepulsed with the corresponding peptide at 1 μM in RPMI 1640 supplemented with 10% human plasma and 200 U/ml human rIL-2).

### *TCR clonotype analysis*

HLA-B*51:01–TI8 tetramers were generated as previously described (7). CTL clones were stained with the tetramers, anti-CD8 mAb, and 7-amino-actinomycin D (7-AAD), and then tetramer$^+$CD8$^+$7-AAD$^-$ cells were sorted by using an FACSAria I (BD Biosciences). The cryopreserved PBMCs from four chronically HIV-1–infected HLA-B*51:01$^+$ individuals were stained with B51-TI8 tetramers, anti-CD8 mAb, and 7-AAD. HLA-B*51:01–TI8 tetramer$^+$ CD8$^+$ 7-AAD$^-$ cells were sorted into 96-well plates (Bio-Rad) by using an FACSAria I (BD Biosciences). For samples from sorted single HLA-B*51:01–TI8-specific CD8$^+$ T cells and CTL clones, unbiased identification of TCR αβ-chain usage was assessed as previously described (8). A modification to the protocol was applied by using illustra ExoStar (GE Healthcare), which contains alkaline phosphatase and exonuclease 1 to remove unincorporated primers and nucleotides from the amplification reaction prior to subsequent steps. For bulk-sorted HLA-B*51:01–TI8-specific CD8$^+$ T cells, TCR genes were cloned with a Zero Blunt TOPO PCR cloning kit (Invitrogen), and then several clones were sequenced. Sequencing was done with a BigDye Terminator v3.1. cycle sequencing kit (Applied Biosystems) and analyzed by ABI 3500 and 3500xL Genetic Analyzer (Applied Biosystems, Carlsbad, CA). All TCR genes are identified using the ImMunoGeneTics database (http://www.imgt.org).

### *Protein expression and purification*

The extracellular domains of 3B TCR α-chain (residues 1–207), 3B TCR β-chain (residues 1–247), and B51 H chain (residues 1–248 ± a biotinylation tag) were inserted into separate pGMT7 expression plasmids for expression under the T7 promoter (9). $\beta_2$-microglobulin (residues 1–247) was similarly expressed. Competent Rosetta DE3 *Escherichia coli* cells were used to produce proteins using 0.5 mM isopropyl β-D-thiogalactoside to induce expression as described previously (9–11). Biotinylated pMHCI was prepared as previously described (12). TCR sequences were engineered to incorporate a nonnatural disulphide bond to aid heterodimerization (9, 13).

### *Surface plasmon resonance experiments*

Surface plasmon resonance (SPR) equilibrium binding analysis was performed using a BIAcore3000 (GE Healthcare Life Sciences) equipped with a CM5 sensor chip as previously reported (12, 14, 15). HLA-A*02:01–ALWGPDPAAA and HLA-B*35:01–VPLRPMTY were used as a negative controls on flow cells 1 and 3 in three separate experiments. SPR equilibrium analyses were carried out to determine the $K_D$ values for the TCR at 25°C in triplicate (representative data shown). For all experiments, ~300 response units pMHC was coupled to the CM5 sensor chip surface. The TCR was then injected at concentrations ranging from 10 times above and 10 times below the known $K_D$ of the interaction at 45 μl/min. The $K_D$ values were calculated assuming 1:1 Langmuir binding ($AB = B^*AB_{MAX}/[K_D + B]$), and the data were analyzed using a global fit algorithm (BIAevaluation 3.1).

### *Crystallization, diffraction data collection, and model refinement*

All protein crystals were grown at 18°C by vapor diffusion via the sitting drop technique. A total of 200 nl 1:1 molar ratio TCR and pMHCI (10 mg/ml) in crystallization buffer (10 mM TRIS [pH 8.1] and 10 mM NaCl) was added to 200 nl reservoir solution. 3B–B51-TI8 crystals were grown in 0.2 M sodium sulfate, 0.1 M BisTris propane (pH 6.5), and 20% w/v PEG 3350 (16). Data were collected at 100 K at the Diamond Light Source (Oxfordshire, U.K.). All datasets were collected at a wavelength of 0.976 Å using an ADSC Q315 CCD detector (Area Detector Systems Corporation). Reflection intensities were estimated with the XIA2 package (17), and the data were scaled, reduced, and analyzed with SCALA and the CCP4 package (18). Structures were solved with molecular replacement using PHASER (19). Sequences were adjusted with COOT (20) and the models refined with REFMAC5. Graphical representations were prepared with PyMOL (21). Data reduction and refinement statistics are shown in Table I. The reflection data and final model coordinates were deposited with the Protein Data Bank database (http://www.rcsb.org) (Protein Data Bank 4MJI).

## Results

### *A public TRAV17/TRBV7-3–encoded TCR dominates responses to B51-TI8*

We first generated TI8-specific CTL clones from seven HLA-B*51:01$^+$HIV$^+$ patients who responded to this epitope. The staining of representative clones by pMHC tetramer with this B51-TI8 epitope is shown in Supplemental Fig. 1. A total of 73 clones were analyzed for their TCRα- and TCRβ-chain sequences by previously described methodology (8). In patients KI-021, KI-127, KI-250, and KI-391, only T cells expressing TCRs with TRAV17/TRBV7-3 genes were detected (Fig. 1A). Patients KI-051 and KI-112 generated CTL clones expressing TRAV17/TRBV7-3 TCRs, but also expressed a further private B51-TI8–specific clonotype. The remaining patient (KI-124) used a completely different TCR made from the TRAV8-6 and TRBV27 genes. Thus, the TRAV17/TRBV7-3 clonotype was exclusively or predominantly detected in six out of seven individuals tested. Importantly, in five of these patients (except KI-391), the TCRα-chain consisted of a TRAV17, TRAJ22, and an identical CDR3 sequence: CATDDDSARQLTF. Curiously, the TCRβ-chain was encoded by a combination of the TRBV7-3, TRBJ2-2, and TRBD2 genes, with CDR3 sequence CASSLTGGELFF, in patients KI-021 and KI-051 (termed the 3B TCR in this study), whereas the TRBJ1-4 and TRBD1 or D2 were used in conjunction with TRBV7-3 in patients KI-112, KI-127, and KI-250 to produce the CDR3 sequence CASSLTGGKLFF (underlining indicates the only amino acid variation between these differentially encoded chains). This convergent evolution suggests that TCRs with this chain may have a strong selective advantage in vivo. A further patient, KI-391, exclusively used a different

Table I. Summary of 3B–B51-TI8 cocomplex structure

| | 3B–B51-TI8 |
|---|---|
| Hydrogen bonds (≤3.2 Å) | 14 |
| Hydrogen bonds (≤3.4 Å) | 4 |
| Vdw (≤3.5 Å) | 37 |
| Vdw (≤4 Å) | 101 |
| Total contacts | 156 |
| No. of α-chain CDR1/CDR2/CDR3 contacts (≤4 Å) | 28/19/46 |
| No. of β-chain CDR1/CDR2/CDR3 contacts (≤4 Å) | 9/41/13 |
| Peptide contacts | 33 |
| MHC contacts | 123 |
| Crossing angle | 43.3° |
| BSA (TCR–MHC) (Å$^2$) | 2041.2 |
| BSA (TCR–peptide) (Å$^2$) | 492.2 |
| BSA (TCR–pMHC) (Å$^2$) | 2533.4 |
| Surface complementarity (TCR–MHC) | 0.6675 |
| Surface complementarity (TCR–peptide) | 0.6675 |
| Surface complementarity (TCR–pMHC) | 0.647 |

**A B51-TI8-specific T cell clones**

| Patient | TRAV | TRAJ | CDR3α | counts of CTL clone or line | TRBV | TRBJ | TRBD | CDR3β | counts of CTL clone or line |
|---|---|---|---|---|---|---|---|---|---|
| KI-021 | V17 | J22 | CATDDDSARQLTF | 15 | V7-3 | J2-2 | D2 | CASSLTGGGELFF | 15 |
| KI-051 | V17 | J22 | CATDDDSARQLTF | 3 | V7-3 | J2-2 | D2 | CASSLTGGGELFF | 3 |
| | V8-2 | J13 | CVVSERAGGYQKV | 7 | V24-1 | J2-1 | D1 | CATSDLQGVRGVNEQF | 7 |
| KI-112 | V17 | J22 | CATDDDSARQLTF | 7 | V7-3 | J1-4 | D1 | CASSLTGGGKLFF | 7 |
| | V29/DV5 | J30 | CAAQRANRDDKIIF | 1 | V11-3 | J2-3 | D2 | CASSPPGGRADTQYF | 1 |
| KI-124 | V8-6 | J53 | CAVSRGGSNYKLTF | 9 | V27 | J2-7 | D2 | CASSSGRGGEQYF | 10 |
| | | J32 | CAVSEGGATNKLIF | 1 | | | | | |
| KI-127 | V17 | J22 | CATDDDSARQLTF | 10 | V7-3 | J1-4 | D1 | CASSLTGGGKLFF | 10 |
| KI-250 | V17 | J22 | CATDDDSARQLTF | 10 | V7-3 | J1-4 | D2 | CASSLTGGGKLFF | 10 |
| KI-391 | V17 | J5 | CATDEAGRRALTF | 10 | V7-3 | J1-3 | D1 | CASSLTGGNTIYF | 10 |

**B *Ex vivo* B51-TI8-specific T cells (bulk analysis)**

| Patient | TRAV | TRAJ | CDR3α | frequency (%) | count | TRBV | TRBJ | TRBD | CDR3β | frequency (%) | count |
|---|---|---|---|---|---|---|---|---|---|---|---|
| KI-021 | V17 | J22 | CATDDDSARQLTF | 100.00 | 15/15 | V7-3 | J2-2 | D2 | CASSLTGGGELFF | 100.00 | 21/21 |
| KI-051 | V17 | J22 | CATDEDSARQLTF | 46.87 | 15/32 | V7-3 | J2-2 | D2 | CASSLTGGGELFF | 59.59 | 13/22 |
| | | | | | | V7-3 | J1-3 | D1 | CASSSTGGNTIYF | 13.63 | 3/22 |
| | | | | | | V7-3 | J1-1 | D2 | CASSLTGNTEAFF | 9.09 | 2/22 |
| | V17 | J5 | CATDDAGRRALTF | 40.63 | 13/32 | V27 | J2-5 | D1 | CASSTRDPRQTQYF | 4.55 | 1/22 |
| | | | | | | V5-1 | J2-5 | D1 | CASSLWLPKETQYF | 4.55 | 1/22 |
| | V5 | J10 | CAERTGGGNKLTF | 12.50 | 4/32 | V12-4 | J2-2 | D1 | CASRKWNGELFF | 4.55 | 1/22 |
| | | | | | | V29-1 | J2-3 | D2 | CSVEGPLAGEADTQYF | 4.55 | 1/22 |
| KI-112 | V29/DV5 | J30 | CAAQRANRDDKIIF | 100.00 | 22/22 | V11-3 | J2-3 | D2 | CASSPPGGRADTQYF | 100.00 | 24/24 |
| KI-124 | V8-6 | J32 | CAVSEGGATNKLIF | 100.00 | 22/22 | V27 | J1-1 | D1 | CASAQGRGTEAFF | 100.00 | 37/37 |

**C *Ex vivo* B51-TI8-specific T cells (single cell sorting)**

| Patient | TRAV | TRAJ | CDR3α | TRBV | TRBJ | TRBD | CDR3β | frequency (%) | count of cell |
|---|---|---|---|---|---|---|---|---|---|
| KI-021 | V17 | J22 | CATDDDSARQLTF | V7-3 | J2-2 | D2 | CASSLTGGGELFF | 88.00 | 22/25 |
| | V12-2 | J16 | CAVTHHGQKLLF | V28 | J2-5 | D2 | CASSSNPIVPQETQYF | 8.00 | 2/25 |
| | V12-2 | J16 | CAVTHHGQKLLF | V4-1 | J1-6 | D1 | CASSRGAESYNSPLHF | 4.00 | 1/25 |
| KI-051 | V17 | J22 | CATDEDSARQLTF | V7-3 | J2-2 | D2 | CASSLTGGGELFF | 44.00 | 8/18 |
| | V17 | J5 | CATDVAGRRALTF | V7-3 | J1-3 | D1 | CASSSTGGNTIYF | 11.00 | 2/18 |
| | V17 | J22 | CATDEDSARQLTF | V7-3 | J2-2 | D2 | CASSLTGGARARLFF | 6.00 | 1/18 |
| | V5 | J10 | CAERTGGGNKLTF | V12-4 | J2-2 | D1 | CASRKWNGELFF | 28.00 | 5/18 |
| | V14/DV4 | J30 | CAMRGPNRDDKIIF | V11-3 | J2-1 | D2 | CASSRRGEGHNEQFF | 11.00 | 2/18 |

**FIGURE 1.** Detection of B51-TI8–specific CTLs expressing public TCRs with the TRAV17/TRBV7-3 genes. (**A**) TCR αβ-chain usage of B51-TI8–specific CTL clones established from seven HLA-B*51:01$^+$ individuals infected with HIV-1. (**B**) Bulk TCR sequence analysis of ex vivo HLA-B*51:01–TI8 tetramer binding CD8$^+$ T cell populations from four of the individuals shown in (A). (**C**) TCR analysis of sorted single cells of ex vivo tetramer binding CD8$^+$ T cells from two patients. TCRs with the TRAV17/TRBV7-3 genes are highlighted in blue. The conserved TCR CDR3α Arg$^{97}$ residue is shown in red.

TCR made from a combination of the TRAV17/TRBJ5 and TRBV7-3/TRBJ1-3 genes. Although the exact sequence of both CDR3 loops differed in KI-391, these loops exhibited an identical length to that seen in all of the other patients (Fig. 1A). In summary, six out of seven patients used the TRAV17/TRBV7-3 TCR (three exclusively).

Examination of T cell clones, as above, could possibly introduce bias due to the ability of only certain clonotypes to proliferate in culture. To control for such potential distortion, we analyzed the clonotype of ex vivo B51-TI8–specific CD8$^+$ T cells from four patients (KI-021, KI-051, KI-112, and KI-124) in whom we could readily gain PBMC samples and sort populations of B51-TI8 tetramer$^+$ CD8$^+$ T cells directly ex vivo. The clonotype of bulk-sorted B51-TI8–specific CD8$^+$ T cells was analyzed for these four patients (Fig. 1B). In accordance with the T cell clone data, only T cells expressing TCRs with TRAV17/TRBV7-3 genes were detected in KI-021. Moreover, TRAV17/TRBV7-3 clonotypes with identical lengths of CDR3α and β loops were also predominantly detected in KI-051. In KI-112, only the TRAV29/DV5/TRBV11-3 clonotype was detected (Fig. 1B), although this clonotype was only expressed in one of eight CTL clones (Fig. 1A). Interestingly, only the TRAV8-6/TRBV27 clonotype was found in all CTL clones (Fig. 1A) and in ex vivo bulk-sorted T cells (Fig. 1B) from KI-124, but different TRAJ, TRBJ, and TRBD were found between two different cell sources. We further performed a single-cell TCR analysis for the samples from KI-021 and KI-051. Paired TCR usage data are shown in Fig. 1C. The TRAV17/TRAJ22/TRBV7-3/TRBJ2-2 clonotype was detected in 22 out of 25 B51-TI8–specific CD8$^+$ T cells sorted from KI-021 PBMCs and 8 out of the 18 CD8$^+$ T cells sorted from KI-051 PBMCs. Interestingly, there was an amino acid difference (Asp-Glu) at position 93 in CDR3α between KI-021 and KI-051 in ex vivo samples but not in CTL clones. TCR analysis for the bulk-cultured T cells from KI-051 used for CTL cloning demonstrated the same TCR sequence as the CTL clones (data not shown), indicating that CTLs carrying the TCR with Asp at position 93 were selected during in vitro stimulation. Thus, TRAV17/TRBV7-3 clonotype was also detected in ex vivo samples from at least two LTNPs (KI-021 and KI-051). These results show that the majority of B51-TI8–specific CTLs express a public TCR with type IV

bias, consisting of a conserved TRBV or TRAV gene, TRBJ or TRAJ gene usage, and only one or two residue differences within the CDR3 loop in multiple individuals (22, 23). The public nature of this TCR the dominance of TI8 responses in HLA-B*51:01$^{+}$ individuals, and the better disease prognosis associated with this allele combine to make the public response especially interesting.

*The 3B TCR binds to B51-TI8 with very weak affinity*

To explore the molecular mechanisms underlying the selective T cell response to B51-TI8, we generated a soluble form of the public TCR (3B) isolated from a CTL clone expressing the TRAV17/TRBV7-3 genes and the common CDR3 loops we detected in our clonotypic analysis (Fig. 1). The affinity of most pathogen-specific TCR–pMHCI interaction lies in the region of $K_D$ = 1–10 μM (24). We used SPR to determine the equilibrium binding affinity of the 3B TCR for B51-TI8. The 3B TCR bound to B51-TI8 with the weakest affinity ever measured for a pathogenic epitope (24), $K_D$ ≈81.8 μM, with kinetics that were too rapid to measure (Fig. 2A). This unusually weak affinity warranted further structure examination of Ag recognition by the public 3B TCR.

*The 3B TCR engages B51-TI8 in classical orientation*

We solved the structure of the 3B–B51-TI8 complex to gain an atomic perspective on the molecular basis for the selection of this public clonotype in response to B51-TI8. The complex was solved to 2.99 Å, and molecular replacement was successful only in space group P1 with statistics consistent with the resolution (Supplemental Table II). Overall, the 3B TCR bound canonically, with the TCR CDRs contacting the pMHC surface (Fig. 2B) in a diagonal docking geometry (43.4°) (Fig. 2C) as previously reported for other TCR–pMHC complexes (25). The 3B TCR broadly contacted the MHC surface (123 total contacts with 22 different MHC residues) with only 33 contacts made between the TCR and peptide (Table I). The contact interface between the 3B TCR and B51-TI8 generated an overall buried surface area (BSA) of 2041.2 Å$^2$ toward the higher end of the observed range for natural TCR–pMHC interactions (25).

*Interactions between the 3B TCR and the restriction triad dominate MHC contacts*

Previous structures of TCR–pMHC complexes have shown that most TCRs use three conserved MHC contact points (positions 65, 69, and 155; the restriction triad) (26, 27). The 3B TCR made a broad contact footprint with the MHC surface, contacting 22 different residues (Fig. 3A, 3B, Supplemental Table III). However, of the 123 interactions between the 3B TCR and the MHC surface, ~40% (49 contacts) were with the restriction triad residues (Gln$^{65}$, Thr$^{69}$, and Gln$^{155}$), including 6 out of 14 hydrogen bonds (Fig. 3C, 3D, Table I). Aside from the restriction triad positions, Arg$^{62}$ (contacting TCR α-chain Asp$^{94}$ and Gln$^{98}$), Gln$^{72}$ (contacting TCR β-chain Gln$^{53}$, Thr$^{55}$, and Gly$^{56}$), and Gln$^{152}$ (contacting TCR α-chain Arg$^{97}$ and β-chain Thr$^{100}$) were the other important MHC contact residues, making a further 24 Van der Waals (Vdw), 1

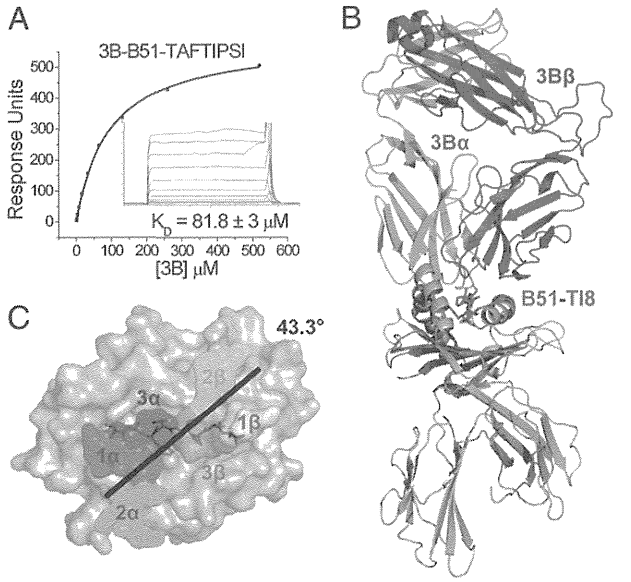


**FIGURE 2.** The 3B TCR binds to B51-TI8 with very weak affinity and engages B51-TI8 in classical orientation. (**A**) 3B TCR binding to B51-TI8. Ten serial dilutions of 3B TCR were measured in three separate experiments (with different protein preparations). Representative data from these experiments are plotted. The equilibrium binding constant ($K_D$) values were calculated using a nonlinear curve fit ($y = [P_1x]/P_2 + x$). Mean plus SD values are shown. To calculate each response, 3B TCR was also injected over a control sample (HLA-A*02:01 in complex with ALWGPDPAAA peptide or HLA-B*35:01 in complex with VPLRPMTY peptide) that was deducted from the experimental data. (**B**) Overall binding mode of the 3B TCR (α-chain in green and β-chain in blue) interacting with B51 (gray) TI8 (red sticks). (**C**) Position and crossing angle of the 3B TCR CDR loops (CDR1α, red; 2α, green; 3α, blue; 1β, yellow; 2β, cyan; 3β, orange) over the B51 (gray surface)-TI8 (red sticks).

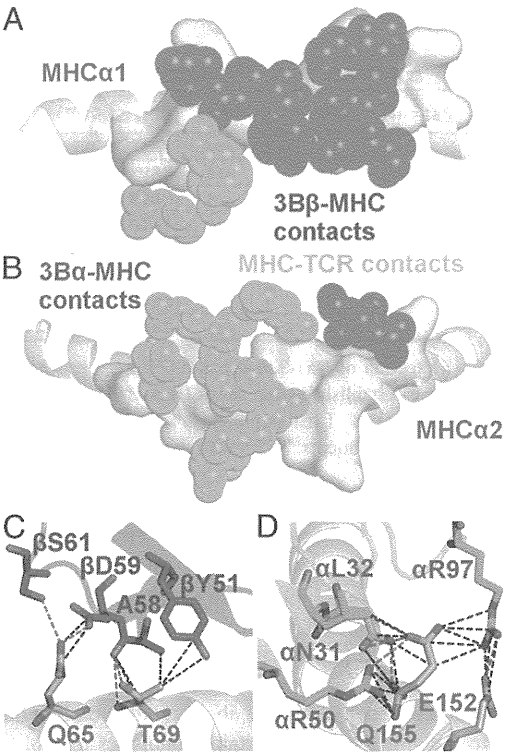


**FIGURE 3.** Interactions between the 3B TCR and the restriction triad dominate MHC contacts. (**A**) Position of the 3B TCR (α in green spheres and β in blue spheres) over the B51 α1 helix (residues contacted by the 3B TCR on the B51 α1 helix shown in yellow surface). (**B**) Position of the 3B TCR (α in green spheres and β in blue spheres) over the B51 α2 helix (residues contacted by the 3B TCR on the B51 α2 helix shown in yellow surface). (**C**) Contacts between the 3B TCR CDR2β loop and the MHCα1 domain including the restriction triad residues Q65 and T69. (**D**) Contacts between the 3B TCR CDR1 and 2α loops and the MHCα2 domain including the restriction triad residue Q155. These important stabilizing interactions include a number of Vdw contacts (black dotted lines, 4 Å cutoff) and hydrogen bonds (red dotted lines, 3.4 Å cutoff) with the MHC surface.

salt-bridge, and 3 hydrogen bonds with the 3B TCR (Supplemental Table III).

*The TI8 peptide lacks the canonical central bulge*

Previous pMHCI structures have shown that the central residues in the peptide generally bulge out of the MHC binding groove mediating TCR contacts (25). The fixed anchors at the N and C termini of the peptide and the closed conformation of the MHCI groove force longer peptides to bulge further out of the groove to accommodate the extra central peptide residues (26). Different T cells have been shown to have a preference for peptides of specific length, presumably dependent on the size of the peptide bulge (28). The 3B–B51-TI8 complex solved in this study is the first ever, to our knowledge, human TCR–pMHCI complex with an 8-mer peptide. The TI8 peptide, being an 8-mer (the shortest length reported for natural MHCI binding peptides) lacked any prominent central bulge and was almost flat in the binding groove, akin to MHC class II peptide presentation (29, 30) (Fig. 4A). The consequences of this flat binding mode were 2-fold. First, the 3B TCR made only 33 contacts with the peptide (Table I), fewer than typically observed for other TCR-pMHCI structures (25). Usually the number of peptide contacts account for ~35% of total contacts rather than the ~25% as seen in this study. Second, the lack of peptide bulge enabled the TCR to form a closer interaction with the MHC surface, supported by the comparatively large BSA of 2041.2 Å observed for the TCR–MHC interface (Table I) (22). These observations demonstrate how the length of the peptide can govern pMHC interactions. For instance, a previously reported TCR–pMHC structure with a superbulged 13-mer peptide showed that the TCR perched on the extended peptide bulge and made limited contacts with the MHC surface (26).

*Peptide positions 4 and 7 are the main contact residues for the 3B TCR*

The 3B TCR contacted six peptide residues in the B51-TI8 complex, with the TCRα-chain contacting peptide residues 3–6 and the TCRβ-chain contacting peptide residues 7 and 8. Despite this broad binding, a total of just 33 interactions were made with the peptide (Fig. 4B) compared with 123 with the MHC, illustrating the MHC-centric nature of the 3B–B51-TI8 interface. The side chains of peptide residues $Thr^4$ and $Ser^7$ were orientated up out of the groove and made the vast majority of the contacts, making all 5 of the hydrogen bonds and 17 of the 28 Vdw interactions between the 3B TCR and the peptide (Fig. 4C). The position of the 3B TCR during binding also demonstrated that, even though there was an amino acid difference (Glu-Lys) at position 104 in CDR3β of TRAV17/TRBV7-3 TCR in KI-112, KI-127, and KI-250, compared with that of the 3B TCR identified in CTL from KI-021 and KI-051, these differences were away from the binding interface of the TCR. Thus, assuming that these two TCRs use a similar binding register, which is likely as they only differ at one residue, they probably use the same molecular mechanism to engage B51-TI8. These data indicate that functionally identical TRAV17/TRBV7-3TCRs were selected in five out of seven HLA-B51:01$^+$HIV$^+$ patients.

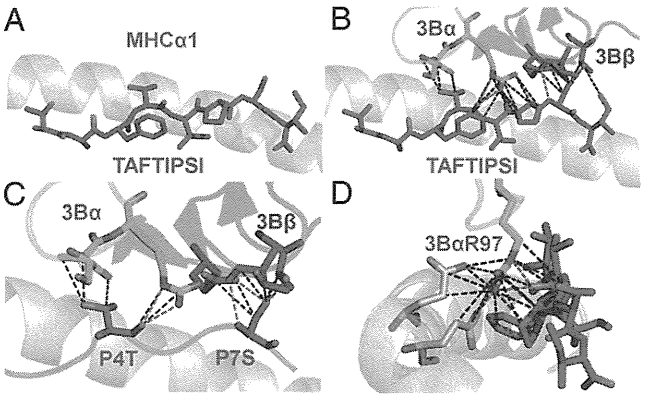


**FIGURE 4.** The TI8 peptide lacks the canonical central bulge. (**A**) Side view of the TI8 peptide (red sticks) conformation demonstrating the lack of a central peptide bulge. (**B**) Contacts between the 3B TCR (α in green sticks and β in blue sticks) and the TI8 peptide (red sticks). (**C**) Contacts between the 3B TCR (α in green sticks and β in blue sticks) and the peptide residues P4T and P7S (red sticks) that represent the majority of interactions between the TCR and peptide. (**D**) Contacts between the 3B TCR CDR3α-chain residue $Arg^{97}$ and the B51 surface (gray sticks) and the TI8 peptide (red sticks). 3B TCR CDR3α-chain residue $Arg^{97}$ interacts with a pocket formed by B51-TI8 in a ball-and-socket–like manner enabling a number of Vdw contacts (black dotted lines, 4Å cutoff) and hydrogen bonds (red dotted lines, 3.4 Å cutoff) to form at the TCR–pMHC interface.

*A conserved binding motif explains public selection of B51-TI8–specific TCRs*

Although the interaction between the 3B TCR and B51-TI8 involved >20 different TCR residues (Supplemental Table III), TCR CDR3α residue $Arg^{97}$ accounted for 3 out of 5 hydrogen bonds and 9 out of 23 Vdw contacts with the peptide and 3 out of 13 hydrogen bonds and 9 out of 110 Vdw contacts with the MHC surface (Fig. 4D). $Arg^{97}$ made this contact network by fitting into a pocket formed by the MHC α2-domain and the peptide backbone, akin to a ball-and-socket joint. Thus, $Arg^{97}$ is likely to be an important driving force in this otherwise weak TCR–pMHCI interaction, acting as an anchor grasping onto both the peptide and MHC. In support of this notion, $Arg^{97}$ was conserved in the CDR3α loops of all of the TRAV17/TRBV7-3 TCRs detected (Fig. 1A), including from patient KI-391 that expressed a distinct CDR3α loop and ex vivo B51-TI8–specific CD8$^+$ T cells in KI-051 (Fig. 1B, 1C). In addition to the dominant role for $Arg^{97}$ in the CDR3α loop, the 3B TCR used a very broad binding motif that included the majority of residues in the TRAV17/TRBV7-3–encoded CDR1 and 2 loops. This additional network of interactions provided a stable binding platform, enabling $Arg^{97}$ to perform its central role and thereby explaining the conservation of this clonotype. Only the combination of the TRAV17 and TRBV7-3 genes encoded for the correct arrangement of residues capable of interacting with B51-TI8 in this mode, probably explaining the predominance of such clonotypes in the B51-TI8 response.

## Discussion

HLA-B*27, HLA-B*51, and HLA-B*57 are associated with better control of HIV infection (3–5). Previous studies with HLA-B*27 and HLA-B*57 have identified residue identical public TCR responses [defined as residue-identical receptors found across different individuals who share a common MHC (22, 31)] against HIV (32–35). For example, public TCR clonotypes were detected in HLA-B*27–restricted p24 Gag-derived KK10-specific (KRWIILGLNK; residues 263–272) CTLs (32, 36). KK10-specific CTLs, characterized by *TRBV4-3/TRBJ1-3* or *TRBV6-5/TRBJ1-1* gene expression, were found to be preferentially selected in vivo and shared between individuals. CTLs expressing this public clonotype exhibited high levels of TCR avidity and Ag sensitivity, enabling functional advantages and effective suppression of HIV-1 replication (32, 36).

We previously demonstrated that the magnitude of B51-TI8–specific CD8$^+$ T cells was significantly correlated to low plasma viral load in chronically HIV-1–infected HLA-B*51:01$^+$ Japanese hemophiliacs (7). No correlation was found between the magnitude of the CD8$^+$ T cell response to three other dominant HLA-B51–

restricted HIV-1 epitopes (7), suggesting that B51-TI8–specific $CD8^+$ T cells might play an important role in the control of viral replication in these patients. In this study, we identified a public CTL clonotype, expressing TRAV17/TRBV7-3 TCR genes, deployed against the immunodominant B51-TI8 epitope. These data indicate that even CTLs having weak TCR affinity could play a central role in the control of HIV-1. The 3B–B51-TI8 structure, which to our knowledge is the first TCR–pMHCI complex structure with the B51 allele and first structure of a human 8-mer peptide TCR–pMHC complex, demonstrated that the conformation of the TI8 peptide was relatively flat compared with the classical prominent central peptide bulge observed for most other pMHCIs. This flat conformation enabled the 3B TCR to bind in an MHC-centric manner, broadly contacting the residues that form the restriction triad. Despite the broad binding mode, a conserved Arg at position 97 in the CDR3α loop dominated contacts and was central to binding. $Arg^{97}$ was also present in patients that used a TCR with a different CDR3α loop, underscoring its central role in the interaction.

Garcia et al. (37) previously solved the crystal structure of the mouse 2C TCR in complex with H-$2K^b$ bound to the 8-mer self-peptide, dEV8 (EQYKFYSV). Analogous to the 3B TCR interaction, the 2C TCR, in complex with H-$2K^b$-dEV8, showed weak affinity ($K_D \approx 84.1$ μM) (38), and the crystal structure of the TCR–pMHC complex revealed that 2C TCR bound in an MHC-centric manner (37). Furthermore, the relative flatness of the TI8 peptide in the binding groove resembles the flat conformation typically observed in pMHC class II (pMHCII) structures (29). Like most TCR–pMHCII complexes, the 3B TCR bound relatively weakly in comparison with the average TCR–pMHCI interaction (24). The structures of the 3B and 2C TCRs suggest a general MHC-centric mode of binding to relatively featureless peptides. The relatively low affinities of 3B and 2C TCRs for their cognate peptides make it tempting to speculate that high-affinity TCRs specific for flatter pMHC landscapes might be deleted during thymic selection because high-affinity MHC-centric TCR binding may increase the potential for cross-reactivity with self. Thus, the weak affinity of the 3B TCR may represent the best B51-TI8 specificity that can escape thymic deletion.

In conclusion, the structure of the 3B TCR in complex with B51-TI8 demonstrates the molecular basis for the selection of this public CTL clonotype in HLA-B*51:01$^+$HIV$^+$ patients by revealing that TCR residues involved in the majority of interactions with the B51-TI8 surface were only encoded by the TRAV17/TRBV7-3 TCR genes. This contact network enabled the conserved $Arg^{97}$ residue in the CDR3α loop to make optimal contacts with B51-TI8 via a ball-and-socket–type interaction. It is also noteworthy that this to our knowledge first ever human TCR–pMHCI structure with an 8-mer peptide, which binds flat within the MHC groove to provide a relatively featureless landscape, showed similarities to the 2C interaction with H-$2K^b$–dEV8 and TCR–pMHCII complexes. All of these TCRs bind to their relatively "vanilla" cognate ligands with weak affinity compared with TCRs that bind to the contoured landscapes of bulging MHCI-restricted foreign peptides of nine or more amino acids in length. We therefore suggest that weak affinity might be a common feature of TCR binding to flat peptides.

## Acknowledgments

We thank the staff at Diamond Light Source for providing facilities and support.

## Disclosures

The authors have no financial conflicts of interest.

## References

1. Davis, M. M., and P. J. Bjorkman. 1988. T-cell antigen receptor genes and T-cell recognition. *Nature* 334: 395–402.
2. Garcia, K. C., L. Teyton, and I. A. Wilson. 1999. Structural basis of T cell recognition. *Annu. Rev. Immunol.* 17: 369–397.
3. Kaslow, R. A., M. Carrington, R. Apple, L. Park, A. Muñoz, A. J. Saah, J. J. Goedert, C. Winkler, S. J. O'Brien, C. Rinaldo, et al. 1996. Influence of combinations of human major histocompatibility complex genes on the course of HIV-1 infection. *Nat. Med.* 2: 405–411.
4. Kiepiela, P., A. J. Leslie, I. Honeyborne, D. Ramduth, C. Thobakgale, S. Chetty, P. Rathnavalu, C. Moore, K. J. Pfafferott, L. Hilton, et al. 2004. Dominant influence of HLA-B in mediating the potential co-evolution of HIV and HLA. *Nature* 432: 769–775.
5. O'Brien, S. J., X. Gao, and M. Carrington. 2001. HLA and AIDS: a cautionary tale. *Trends Mol. Med.* 7: 379–381.
6. Kawashima, Y., K. Pfafferott, J. Frater, P. Matthews, R. Payne, M. Addo, H. Gatanaga, M. Fujiwara, A. Hachiya, H. Koizumi, et al. 2009. Adaptation of HIV-1 to human leukocyte antigen class I. *Nature* 458: 641–645.
7. Kawashima, Y., N. Kuse, H. Gatanaga, T. Naruto, M. Fujiwara, S. Dohki, T. Akahoshi, K. Maenaka, P. Goulder, S. Oka, and M. Takiguchi. 2010. Long-term control of HIV-1 in hemophiliacs carrying slow-progressing allele HLA-B*5101. *J. Virol.* 84: 7151–7160.
8. Sun, X., M. Saito, Y. Sato, T. Chikata, T. Naruto, T. Ozawa, E. Kobayashi, H. Kishi, A. Muraguchi, and M. Takiguchi. 2012. Unbiased analysis of TCRα/β chains at the single-cell level in human CD8+ T-cell subsets. *PLoS ONE* 7: e40386.
9. Garboczi, D. N., P. Ghosh, U. Utz, Q. R. Fan, W. E. Biddison, and D. C. Wiley. 1996. Structure of the complex between human T-cell receptor, viral peptide and HLA-A2. *Nature* 384: 134–141.
10. Cole, D. K., S. M. Dunn, M. Sami, J. M. Boulter, B. K. Jakobsen, and A. K. Sewell. 2008. T cell receptor engagement of peptide-major histocompatibility complex class I does not modify CD8 binding. *Mol. Immunol.* 45: 2700–2709.
11. Cole, D. K., P. J. Rizkallah, F. Gao, N. I. Watson, J. M. Boulter, J. I. Bell, M. Sami, G. F. Gao, and B. K. Jakobsen. 2006. Crystal structure of HLA-A*2402 complexed with a telomerase peptide. *Eur. J. Immunol.* 36: 170–179.
12. Wyer, J. R., B. E. Willcox, G. F. Gao, U. C. Gerth, S. J. Davis, J. I. Bell, P. A. van der Merwe, and B. K. Jakobsen. 1999. T cell receptor and coreceptor CD8 alphaalpha bind peptide-MHC independently and with distinct kinetics. *Immunity* 10: 219–225.
13. Boulter, J. M., M. Glick, P. T. Todorov, E. Baston, M. Sami, P. Rizkallah, and B. K. Jakobsen. 2003. Stable, soluble T-cell receptor molecules for crystallization and therapeutics. *Protein Eng.* 16: 707–711.
14. Cole, D. K., P. J. Rizkallah, J. M. Boulter, M. Sami, A. L. Vuidepot, M. Glick, F. Gao, J. I. Bell, B. K. Jakobsen, and G. F. Gao. 2007. Computational design and crystal structure of an enhanced affinity mutant human CD8 alphaalpha coreceptor. *Proteins* 67: 65–74.
15. Gostick, E., D. K. Cole, S. L. Hutchinson, L. Wooldridge, S. Tafuro, B. Laugel, A. Lissina, A. Oxenius, J. M. Boulter, D. A. Price, and A. K. Sewell. 2007. Functional and biophysical characterization of an HLA-A*6801-restricted HIV-specific T cell receptor. *Eur. J. Immunol.* 37: 479–486.
16. Bulek, A. M., F. Madura, A. Fuller, C. J. Holland, A. J. Schauenburg, A. K. Sewell, P. J. Rizkallah, and D. K. Cole. 2012. TCR/pMHC Optimized Protein crystallization Screen. *J. Immunol. Methods* 382: 203–210.
17. Winter, G. 2010. *xia2*: an expert system for macromolecular crystallography data reduction. *J. Appl. Cryst.* 43: 186–190.
18. Collaborative Computational Project, Number 4. 1994. The CCP4 suite: programs for protein crystallography. *Acta Crystallogr. D Biol. Crystallogr.* 50: 760–763.
19. McCoy, A. J., R. W. Grosse-Kunstleve, P. D. Adams, M. D. Winn, L. C. Storoni, and R. J. Read. 2007. Phaser crystallographic software. *J. Appl. Cryst.* 40: 658–674.
20. Emsley, P., and K. Cowtan. 2004. Coot: model-building tools for molecular graphics. *Acta Crystallogr. D Biol. Crystallogr.* 60: 2126–2132.
21. Delano, W. L. 2002. *The PyMOL Molecular Graphics System.* DeLano Scientific, San Carlos, CA.
22. Miles, J. J., A. M. Bulek, D. K. Cole, E. Gostick, A. J. Schauenburg, G. Dolton, V. Venturi, M. P. Davenport, M. P. Tan, S. R. Burrows, et al. 2010. Genetic and structural basis for selection of a ubiquitous T cell receptor deployed in Epstein-Barr virus infection. *PLoS Pathog.* 6: e1001198.
23. Miles, J. J., D. C. Douek, and D. A. Price. 2011. Bias in the αβ T-cell repertoire: implications for disease pathogenesis and vaccination. *Immunol. Cell Biol.* 89: 375–387.
24. Cole, D. K., N. J. Pumphrey, J. M. Boulter, M. Sami, J. I. Bell, E. Gostick, D. A. Price, G. F. Gao, A. K. Sewell, and B. K. Jakobsen. 2007. Human TCR-binding affinity is governed by MHC class restriction. *J. Immunol.* 178: 5727–5734.
25. Rudolph, M. G., R. L. Stanfield, and I. A. Wilson. 2006. How TCRs bind MHCs, peptides, and coreceptors. *Annu. Rev. Immunol.* 24: 419–466.
26. Tynan, F. E., S. R. Burrows, A. M. Buckle, C. S. Clements, N. A. Borg, J. J. Miles, T. Beddoe, J. C. Whisstock, M. C. Wilce, S. L. Silins, et al. 2005. T cell receptor recognition of a 'super-bulged' major histocompatibility complex class I-bound peptide. *Nat. Immunol.* 6: 1114–1122.
27. Gras, S., S. R. Burrows, S. J. Turner, A. K. Sewell, J. McCluskey, and J. Rossjohn. 2012. A structural voyage toward an understanding of the MHC-I-restricted immune response: lessons learned and much to be learned. *Immunol. Rev.* 250: 61–81.

28. Ekeruche-Makinde, J., J. J. Miles, H. A. van den Berg, A. Skowera, D. K. Cole, G. Dolton, A. J. Schauenburg, M. P. Tan, J. M. Pentier, S. Llewellyn-Lacey, et al. 2013. Peptide length determines the outcome of TCR/peptide-MHCI engagement. *Blood* 121: 1112–1123.
29. Stern, L. J., J. H. Brown, T. S. Jardetzky, J. C. Gorga, R. G. Urban, J. L. Strominger, and D. C. Wiley. 1994. Crystal structure of the human class II MHC protein HLA-DR1 complexed with an influenza virus peptide. *Nature* 368: 215–221.
30. Holland, C. J., D. K. Cole, and A. Godkin. 2013. Re-directing CD4(+) T cell responses with the flanking residues of MHC class II-bound peptides: the core is not enough. *Front. Immunol.* 4: 172.
31. Turner, S. J., P. C. Doherty, J. McCluskey, and J. Rossjohn. 2006. Structural determinants of T-cell receptor bias in immunity. *Nat. Rev. Immunol.* 6: 883–894.
32. Iglesias, M. C., J. R. Almeida, S. Fastenackels, D. J. van Bockel, M. Hashimoto, V. Venturi, E. Gostick, A. Urrutia, L. Wooldridge, M. Clement, et al. 2011. Escape from highly effective public CD8+ T-cell clonotypes by HIV. *Blood* 118: 2138–2149.
33. Gillespie, G. M., G. Stewart-Jones, J. Rengasamy, T. Beattie, J. J. Bwayo, F. A. Plummer, R. Kaul, A. J. McMichael, P. Easterbrook, T. Dong, et al. 2006. Strong TCR conservation and altered T cell cross-reactivity characterize a B*57-restricted immune response in HIV-1 infection. *J. Immunol.* 177: 3893–3902.
34. Yu, X. G., M. Lichterfeld, S. Chetty, K. L. Williams, S. K. Mui, T. Miura, N. Frahm, M. E. Feeney, Y. Tang, F. Pereyra, et al. 2007. Mutually exclusive T-cell receptor induction and differential susceptibility to human immunodeficiency virus type 1 mutational escape associated with a two-amino-acid difference between HLA class I subtypes. *J. Virol.* 81: 1619–1631.
35. Chen, H., Z. M. Ndhlovu, D. Liu, L. C. Porter, J. W. Fang, S. Darko, M. A. Brockman, T. Miura, Z. L. Brumme, A. Schneidewind, et al. 2012. TCR clonotypes modulate the protective effect of HLA class I molecules in HIV-1 infection. *Nat. Immunol.* 13: 691–700.
36. Ladell, K., M. Hashimoto, M. C. Iglesias, P. G. Wilmann, J. E. McLaren, S. Gras, T. Chikata, N. Kuse, S. Fastenackels, E. Gostick, et al. 2013. A molecular basis for the control of preimmune escape variants by HIV-specific CD8+ T cells. *Immunity* 38: 425–436.
37. Garcia, K. C., M. Degano, L. R. Pease, M. Huang, P. A. Peterson, L. Teyton, and I. A. Wilson. 1998. Structural basis of plasticity in T cell receptor recognition of a self peptide-MHC antigen. *Science* 279: 1166–1172.
38. Garcia, K. C., M. D. Tallquist, L. R. Pease, A. Brunmark, C. A. Scott, M. Degano, E. A. Stura, P. A. Peterson, I. A. Wilson, and L. Teyton. 1997. Alphabeta T cell receptor interactions with syngeneic and allogeneic ligands: affinity measurements and crystallization. *Proc. Natl. Acad. Sci. USA* 94: 13838–13843.

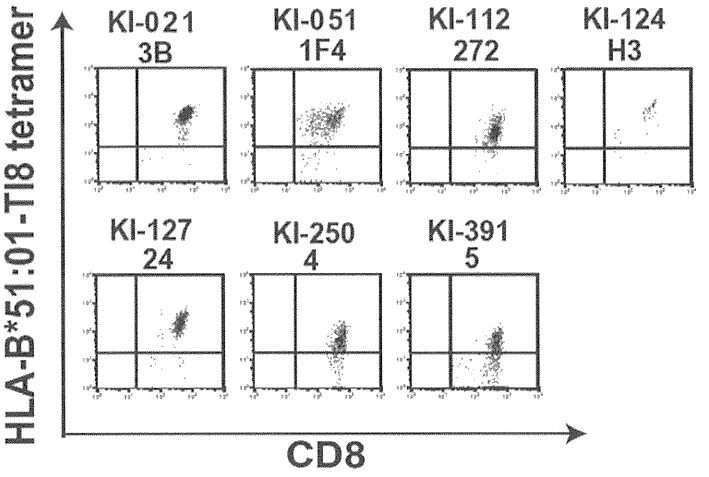


Supplemental Figure 1

**Supplementary Figure 1: HLA-B*51:01-TI8-tetramer$^{+}$CD8$^{+}$ CTL clones**
HLA-B*51:01-restricted TI8-specific CTL clones were stained with the tetramers, anti-CD8 mAb, and 7-AAD, and then analyzed by FACS Aria. Data of a representative CTL clone from each patient are shown. Tetramers$^{+}$CD8$^{+}$ T cell populations among 7-AAD$^{-}$ cells were sorted and then used for TCR clonotypic analysis.